Electronic Supplementary Information: The Role of A-Cations in the Polymorphic Stability and Optoelectronic Properties of Lead-free $ASnI_3$ Perovskites

Mailde S. Ozório,* Srikanth Malladi,* Rafael Besse,* and Juarez L. F. Da Silva*

São Carlos Institute of Chemistry, University of São Paulo, PO Box 780, 13560 − 970, *São Carlos, SP, Brazil*

E-mail: mailde.s.ozorio@usp.br; smalladi@usp.br; rafael.besse@usp.br; juarez_dasilva@iqsc.usp.br

Contents

1 Introduction

In this electronic supporting information, we report the definition for the structural parameters, computational convergence calculations, and additional data for all the studied systems and properties. Furthermore, additional information can be obtained directly with the authors by e-mail.

2 Structural, Energetic and Optical Parameters Definitions

The tin effective coordination number was obtained by the following equation,

$$\mathrm{ECN}^{\mathrm{Sn}} = \sum_j \exp\left[1 - \left(\frac{d_{ij}}{d^i_{av}}\right)^6\right], \qquad d^i_{av} = \frac{\sum_j d_{ij} \exp\left[1 - \left(\frac{d_{ij}}{d_{\min}}\right)^6\right]}{\sum_j \exp\left[1 - \left(\frac{d_{ij}}{d_{\min}}\right)^6\right]}, \tag{1}$$

where d_{ij} is the Sn−I bond-length of octahedra, d^i_{av} a weighted average bond length, and $d_{\min}$ the shortest Sn−I bond lenght of octahedron.

The cohesive energy was achieved by the following equation,

$$E_{coh} = \frac{E(A\mathrm{SnI}_{3(\mathrm{s})}) - \sum \nu E_X}{Z}, \tag{2}$$

where E_X indicates the total energy in eV/atom of each ν free atom X contained in the $A\mathrm{SnI}_3$ bulk with Z formula-unit per cell.

The absorption coefficient, $\alpha(\omega)$, was obtained by the following equation,

$$\alpha(\omega) = \frac{\sqrt{2}\omega}{c}\left[\sqrt{\epsilon_1^2 + \epsilon_2^2} - \epsilon_1\right]^{\frac{1}{2}} \tag{3}$$

where, ω represent the incident photon frequency, c is the speed of light, while ϵ_1^1 and ϵ_1^2 represent, respectively, the real and imaginary parts of the dielectric function.

3 Computational Convergence Tests

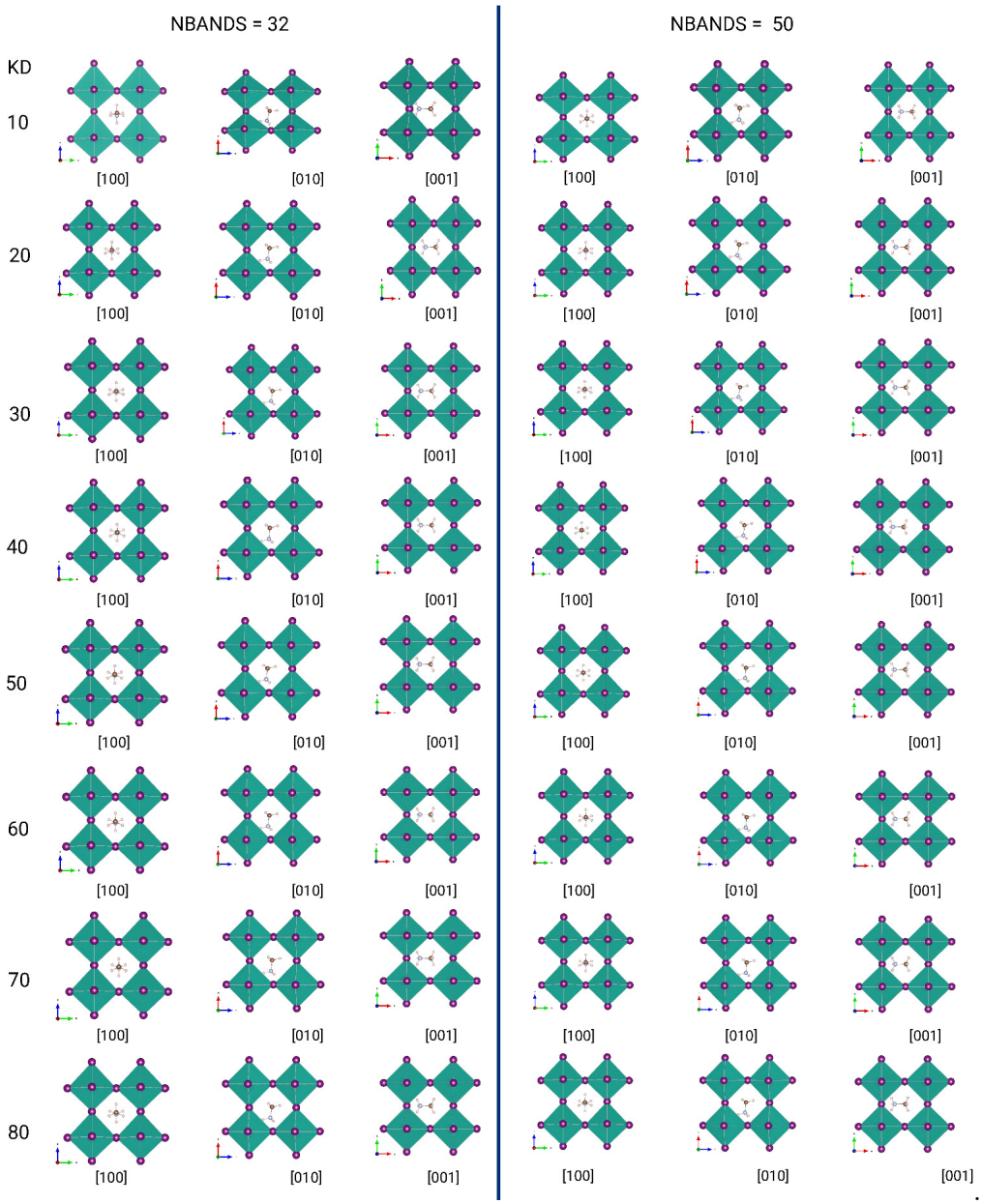

Figure S1 Orientation of the organic cation C−N bond in the cage formed by octahedra.

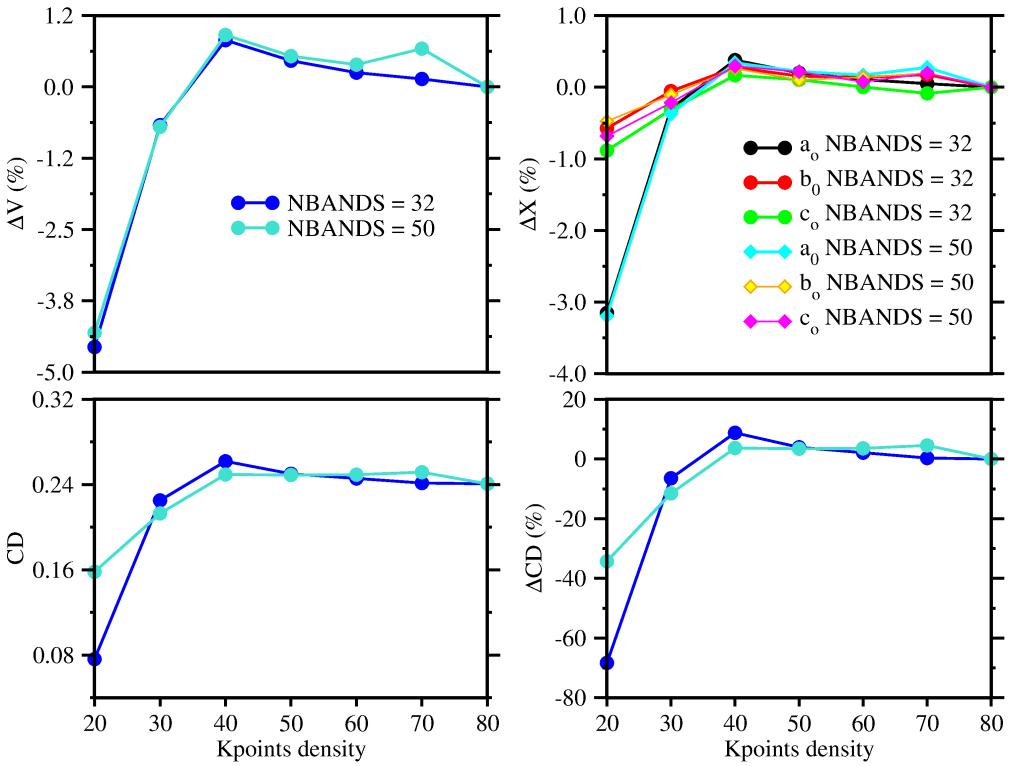

Figure S2 PBE results for $CH_3NH_3SnI_3$ volume, lattice parameters, and cubic deviation in relation to the highest kpoints density.

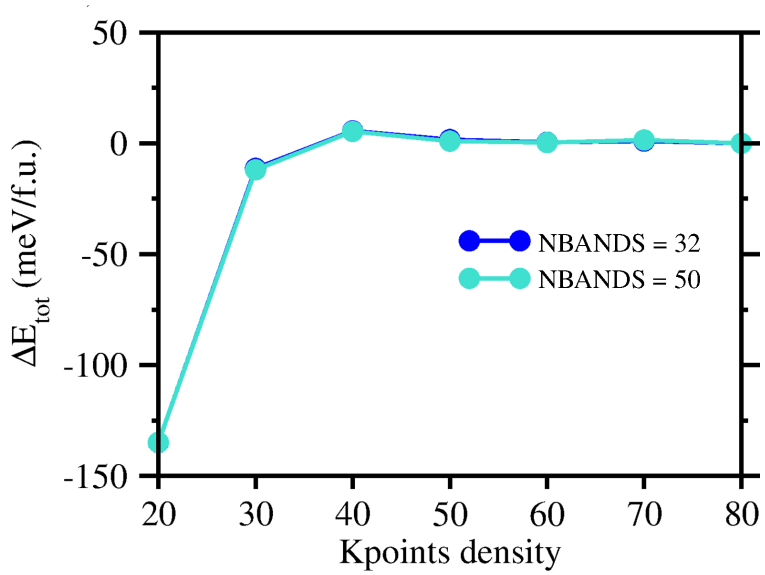

Figure S3 PBE results for $CH_3NH_3SnI_3$ relative total energy to the energy of highest k-points density.

Table S1 Cubic $CH_3NH_3SnI_3$ perovskites: k points density (KD), k-points mesh (KM), number of k-points (NK), volume (V), cubic volume (a_0^c), lattice parameters (a_0, b_0, b_0), cubic deviation (CD) and the relative deviation (considering all significant numbers) of aforementioned parameters in relation to the highest k-points density.

1-16	KD	KM	NK	V (Å^3)	ΔV (%)	a_0^c (Å)	Δa_0^c (%)	CD (Å)	ΔCD (%)	a_0 (Å)	Δa_0 (%)	b_0 (Å	Δb_0 (%)	c_0 (Å)	Δc_0 (%)
NBANDS = 32	10	$1 \times 2 \times 1$	2	242.66	−8.48	6.24	−2.91	1.96	715.91	5.98	−10.60	6.79	4.90	5.97	7.98
	20	$3 \times 3 \times 3$	10	253.05	−4.56	6.33	−1.54	0.08	−68.33	6.30	−3.15	6.30	−0.57	6.38	−0.88
	30	$5 \times 5 \times 5$	39	263.37	−0.67	6.41	−0.22	0.23	−6.46	6.49	−0.30	6.33	−0.05	6.41	−0.31
	40	$6 \times 6 \times 6$	80	267.32	0.82	6.44	0.27	0.26	8.78	6.53	0.38	6.35	0.28	6.44	0.17
	50	$8 \times 8 \times 8$	170	266.36	0.46	6.43	0.15	0.25	3.92	6.52	0.20	6.35	0.16	6.44	0.10
	60	$9 \times 9 \times 9$	205	265.80	0.25	6.43	0.08	0.25	2.12	6.51	0.11	6.35	0.14	6.43	0.00
	70	$11 \times 11 \times 11$	366	265.51	0.14	6.43	0.05	0.24	0.31	6.51	0.05	6.35	0.18	6.43	−0.09
	80	$12 \times 13 \times 12$	518	265.14	0.00	6.42	0.00	0.24	0.00	6.50	0.00	6.34	0.00	6.43	0.00
NBANDS = 50	10	$1 \times 2 \times 1$	2	242.67	−8.31	6.24	−2.85	0.81	237.31	5.98	−8.05	6.78	7.04	5.98	−6.84
	20	$3 \times 3 \times 3$	10	253.27	−4.31	6.33	−1.46	0.16	−34.30	6.29	−3.19	6.31	−0.47	6.38	−0.68
	30	$5 \times 5 \times 5$	39	262.83	−0.70	6.41	−0.23	0.21	−11.54	6.48	−0.37	6.33	−0.11	6.41	−0.22
	40	$6 \times 6 \times 6$	80	267.07	0.91	6.44	0.30	0.25	3.66	6.52	0.34	6.35	0.26	6.44	0.30
	50	$8 \times 8 \times 8$	170	266.09	0.54	6.43	0.18	0.25	3.44	6.52	0.22	6.34	0.10	6.44	0.21
	60	$9 \times 9 \times 9$	205	265.69	0.39	6.43	0.13	0.25	3.57	6.51	0.17	6.35	0.14	6.43	0.07
	70	$11 \times 11 \times 11$	366	266.45	0.67	6.43	0.25	0.25	4.55	6.52	0.28	6.35	0.20	6.44	0.19
	80	$12 \times 13 \times 12$	518	264.67	0.00	6.42	0.00	0.24	0.00	6.50	0.00	6.34	0.00	6.42	0.00

Table S3 Orthorhombic hybrid $CH_3NH_3SnI_3$ perovskites optimization: k-points density (KD), k-points mesh (KM), Number of k-points (NK), volume (V), lattice parameters (a_0, b_0, b_0), and the relative deviation (considering all significant numbers) of aforementioned parameters in relation to the highest k-pints density.

KD	KM	NK	V (Å^3)	ΔV (%)	a_0 (Å)	Δa_0 (%)	b_0 (Å	Δb_0 (%)	c_0 (Å)	Δc_0 (%)
10	$1 \times 1 \times 1$	1	1025.71	3.49	9.29	1.23	13.27	4.87	8.32	−2.52
20	$2 \times 2 \times 2$	8	996.53	0.54	9.17	−0.08	12.70	0.42	8.55	0.19
30	$3 \times 2 \times 4$	12	993.22	0.21	9.18	−0.03	12.69	0.31	8.53	−0.07
40	$4 \times 3 \times 5$	18	991.50	0.04	9.17	−0.07	12.66	0.09	8.54	0.02
50	$5 \times 4 \times 6$	36	991.01	−0.01	9.18	0.06	12.66	0.09	8.52	−0.16
60	$7 \times 5 \times 7$	48	991.13	0.00	9.18	0.00	12.65	0.00	8.54	0.00

Table S2 Cubic hybrid $CH_3NH_3SnI_3$ perovskites optimization: relative total energy, ΔE_{tot}, average, $d^N_{\mathrm{I-H}}$, and standard deviation ($\sigma^N_{\mathrm{I-H}}$) of stronger hydrogen bond of $-NH_3{}^+$ group, average ($d^C_{\mathrm{I-H}}$) and standard deviation ($\sigma^C_{\mathrm{I-H}}$) of stronger hydrogen bond of $-CH_3$ group, difference of the average hydrogen bonds of $-NH_3{}^+$ and $-CH_3$, $\Delta d_{\mathrm{I-H}}$, effective coordination number, $\mathrm{ECN^{Sn}}$, average, $d^{\mathrm{Sn-I}}_{av}$, and standard deviation of Sn−I bond lengths, $\sigma^{\mathrm{Sn-I}}$, octahedra diagonal I−Sn−I angle, Θ, and standard deviation, σ^{Θ}, adjacent I−Sn−I angle, θ, and standard deviation, σ^{θ}, distortion index (DI), and bond angle variance (BAV).

	KD	ΔE_{tot}	$d^N_{\mathrm{I-H}}$	$\sigma^N_{\mathrm{I-H}}$	$d^C_{\mathrm{I-H}}$	$\sigma^C_{\mathrm{I-H}}$	$\Delta d_{\mathrm{I-H}}$	$\mathrm{ECN^{Sn}}$	$d^{\mathrm{Sn-I}}_{av}$	$\sigma^{\mathrm{Sn-I}}$	Θ	σ^{Θ}	θ	σ^{θ}	DI	BAV
	($\mathrm{Å}^{-1}$)	(meV)	(Å)	(Å)	(Å)	(Å)	(Å)	(NNN)	(Å)	(Å)	(deg.)	(deg.)	(deg.)	(deg.)	-	(deg.)^2
NBANDS = 32	10	−2452.15	2.82	0.29	3.24	0.25	0.43	5.22	3.13	0.21	178.27	2.03	90.00	1.25	0.06	1.56
	20	−134.90	2.69	0.06	3.41	0.01	0.72	5.91	3.16	0.07	175.70	0.96	89.99	2.28	0.02	5.21
	30	−11.31	2.69	0.06	3.53	0.03	0.84	5.05	3.21	0.21	171.69	4.14	89.85	4.70	0.05	22.09
	40	5.60	2.69	0.08	3.52	0.10	0.83	4.76	3.23	0.24	171.11	4.69	89.82	5.07	0.06	25.77
	50	1.69	2.68	0.08	3.52	0.10	0.83	4.84	3.23	0.23	171.27	4.27	89.84	4.93	0.05	24.30
	60	0.43	2.69	0.07	3.52	0.08	0.84	4.88	3.23	0.23	171.25	4.20	89.84	4.93	0.05	24.30
	70	1.05	2.69	0.07	3.51	0.08	0.82	4.88	3.22	0.23	171.23	4.36	89.83	4.96	0.05	24.63
	80	0.00	2.69	0.06	3.55	0.05	0.86	4.91	3.22	0.23	171.03	4.08	89.83	5.02	0.05	25.18
NBANDS = 50	10	−2463.64	2.79	0.27	3.27	0.27	0.48	5.23	3.13	0.21	177.40	3.15	90.01	1.91	0.06	3.64
	20	−134.85	2.69	0.06	3.41	0.01	0.72	5.92	3.17	0.06	175.98	0.66	89.99	2.12	0.02	4.48
	30	−11.93	2.69	0.06	3.53	0.03	0.84	5.09	3.21	0.20	171.55	4.11	89.85	4.76	0.04	22.66
	40	5.35	2.69	0.08	3.51	0.11	0.82	4.77	3.23	0.24	170.92	4.50	89.82	5.13	0.06	26.39
	50	0.96	2.69	0.07	3.53	0.08	0.84	4.84	3.23	0.23	170.78	4.38	89.82	5.18	0.05	26.90
	60	0.36	2.69	0.08	3.53	0.07	0.83	4.88	3.23	0.23	171.29	4.41	89.83	4.94	0.05	24.41
	70	1.49	2.69	0.08	3.50	0.11	0.81	4.83	3.23	0.23	171.43	4.41	89.84	4.87	0.05	23.76
	80	0.00	2.69	0.06	3.52	0.06	0.83	4.95	3.22	0.22	170.89	4.09	89.84	5.08	0.05	25.79

Table S4 Orthorhombic hybrid $CH_3NH_3SnI_3$ perovskites optimization: relative total energy (ΔE_{tot}), average ($d^N_{\mathrm{I-H}}$) and standard deviation ($\sigma^N_{\mathrm{I-H}}$) of stronger hydrogen bond of $-NH_3{}^+$ group, average ($d^C_{\mathrm{I-H}}$) and standard deviation ($\sigma^C_{\mathrm{I-H}}$) of stronger hydrogen bond of $-CH_3$ group, difference of the average hydrogen bonds of $-NH_3{}^+$ and $-CH_3$ ($\Delta d_{\mathrm{I-H}}$), octahedra effective coordination number ($\mathrm{ECN^{Sn}}$), average ($d^{\mathrm{Sn-I}}_{av}$) and standard deviation of Sn−I bond lengths ($\sigma^{\mathrm{Sn-I}}$), octahedra diagonal I−Sn−I angle (Θ) and standard deviation (σ^{Θ}), octahedra adjacent I−Sn−I angle (θ) and standard deviation (σ^{θ}), distortion index (DI), and bond angle variance (BAV).

	KD	ΔE_{tot}	$d^N_{\mathrm{I-H}}$	$\sigma^N_{\mathrm{I-H}}$	$d^C_{\mathrm{I-H}}$	$\sigma^C_{\mathrm{I-H}}$	$\Delta d_{\mathrm{I-H}}$	$\mathrm{ECN^{Sn}}$	$d^{\mathrm{Sn-I}}_{av}$	$\sigma^{\mathrm{Sn-I}}$	Θ	σ^{Θ}	θ	σ^{θ}	DI	BAV
	($\mathrm{Å}^{-1}$)	(meV)	(Å)	(Å)	(Å)	(Å)	(Å)	(NNN)	(Å)	(Å)	(deg.)	(deg.)	(deg.)	(deg.)	-	$(\mathrm{deg.})^2$
NBANDS = 126	10	2718.66	2.68	0.07	3.16	0.02	0.47	5.99	3.32	0.02	180.00	0.00	90.00	8.09	0.00	59.47
	20	166.40	2.64	0.01	3.23	0.13	0.60	6.00	3.21	0.01	180.00	0.00	90.00	2.74	0.00	6.82
	30	51.41	2.65	0.01	3.25	0.12	0.60	6.00	3.20	0.01	180.00	0.00	90.00	2.77	0.00	6.98
	40	5.57	2.65	0.02	3.24	0.13	0.59	6.00	3.20	0.01	180.00	0.00	90.00	2.62	0.00	6.24
	50	1.14	2.66	0.01	3.24	0.11	0.58	6.00	3.20	0.01	180.00	0.00	90.00	2.68	0.00	6.55
	60	0.00	2.66	0.00	3.25	0.11	0.59	6.00	3.20	0.01	180.00	0.00	90.00	2.61	0.00	6.20

Table S5 ENCUT analysis (NBANDS default) for cubic hybrid $CH_3NH_3SnI_3$ perovskites optimization: k-points mesh (KM), Number of k-points (NK), volume (V), cubic volume (a^c_0), lattice parameters (a_0, b_0, b_0), relative total energy (ΔE_{tot}), cubic deviation (CD) and the relative deviation of aforementioned parameters in relation to the highest k-pints density.

ENCUT	KM	NK	V	ΔV	a^c_0	Δa^c_0	CD	ΔCD	a_0	Δa_0	b_0	Δb_0	c_0	Δc_0
(eV)			($\mathrm{Å}^3$)	(%)	(Å)	(%)	(Å)	(%)	(Å)	(%)	(Å	(%)	(Å)	(%)
421	$6\times6\times6$	80	243.05	−9.13	6.24	−3.10	0.07	−73.07	6.25	−4.29	6.20	−2.36	6.27	−2.79
526	$6\times6\times6$	80	260.09	−2.76	6.38	−0.93	0.15	−42.31	6.43	−1.53	6.32	−0.47	6.39	−0.93
631	$6\times6\times6$	80	263.33	−1.55	6.41	−0.46	0.24	−0.08	6.49	−0.61	6.33	−0.31	6.41	−0.06
737	$6\times6\times6$	80	266.25	−0.46	6.43	−0.16	0.26	0.00	6.52	−0.15	6.35	0.00	6.43	−0.31
842	$6\times6\times6$	80	267.32	−0.06	6.44	0.00	0.27	3.85	6.53	0.00	6.35	0.00	6.44	−0.16
947	$6\times6\times6$	80	268.21	0.27	6.45	0.16	0.28	7.69	6.54	0.15	6.36	0.16	6.45	0.00
1053	$6\times6\times6$	80	267.48	0.00	6.44	0.00	0.26	0.00	6.53	0.00	6.35	0.00	6.45	0.00

Table S6 ENCUT test (NBANDS default) for cubic hybrid $CH_3NH_3SnI_3$ perovskites optimization: relative total energy (ΔE_{tot}), average ($d^N_{\mathrm{I-H}}$) and standard deviation ($\sigma^N_{\mathrm{I-H}}$) of stronger hydrogen bond of $-NH_3{}^+$ group, average ($d^C_{\mathrm{I-H}}$) and standard deviation ($\sigma^C_{\mathrm{I-H}}$) of stronger hydrogen bond of $-CH_3$ group, difference of the average hydrogen bonds of $-NH_3{}^+$ and $-CH_3$ ($\Delta d_{\mathrm{I-H}}$), octahedra effective coordination number ($\mathrm{ECN^{Sn}}$), average ($d^{\mathrm{Sn-I}}_{av}$) and standard deviation of Sn−I bond lengths ($\sigma^{\mathrm{Sn-I}}$), octahedra diagonal I−Sn−I angle (Θ) and standard deviation (σ^{Θ}), octahedra adjacent I−Sn−I angle (θ) and standard deviation (σ^{θ}), distortion index (DI), and bond angle variance (BAV).

ENCUT	ΔE_{tot}	$d^N_{\mathrm{I-H}}$	$\sigma^N_{\mathrm{I-H}}$	$d^C_{\mathrm{I-H}}$	$\sigma^C_{\mathrm{I-H}}$	$\Delta d_{\mathrm{I-H}}$	$\mathrm{ECN^{Sn}}$	$d^{\mathrm{Sn-I}}_{av}$	$\sigma^{\mathrm{Sn-I}}$	Θ	σ^{Θ}	θ	σ^{θ}	DI	BAV
	(meV)	(Å)	(Å)	(Å)	(Å)	(Å)	(NNN)	(Å)	(Å)	(deg.)	(deg.)	(deg.)	(deg.)	-	(deg.)^2
421	208.83	2.67	0.01	3.30	0.02	0.63	5.78	3.13	0.10	171.20	2.40	89.94	4.71	0.02	22.23
526	36.98	2.68	0.07	3.47	0.05	0.79	5.15	3.20	0.19	171.29	4.01	89.85	4.87	0.04	23.75
631	10.70	2.69	0.06	3.53	0.04	0.84	4.99	3.22	0.22	170.87	4.10	89.83	5.09	0.05	25.98
737	4.73	2.69	0.09	3.49	0.11	0.81	4.99	3.22	0.22	171.15	4.65	89.82	5.05	0.05	25.98
842	2.08	2.69	0.08	3.52	0.10	0.83	4.76	3.23	0.24	171.11	4.69	89.82	5.07	0.06	25.77
947	1.93	2.69	0.09	3.51	0.12	0.82	4.69	3.24	0.25	171.28	4.86	89.81	5.02	0.06	25.27
1053	0.00	2.69	0.08	3.53	0.10	0.84	4.75	3.23	0.24	171.07	4.34	89.82	5.04	0.06	25.40

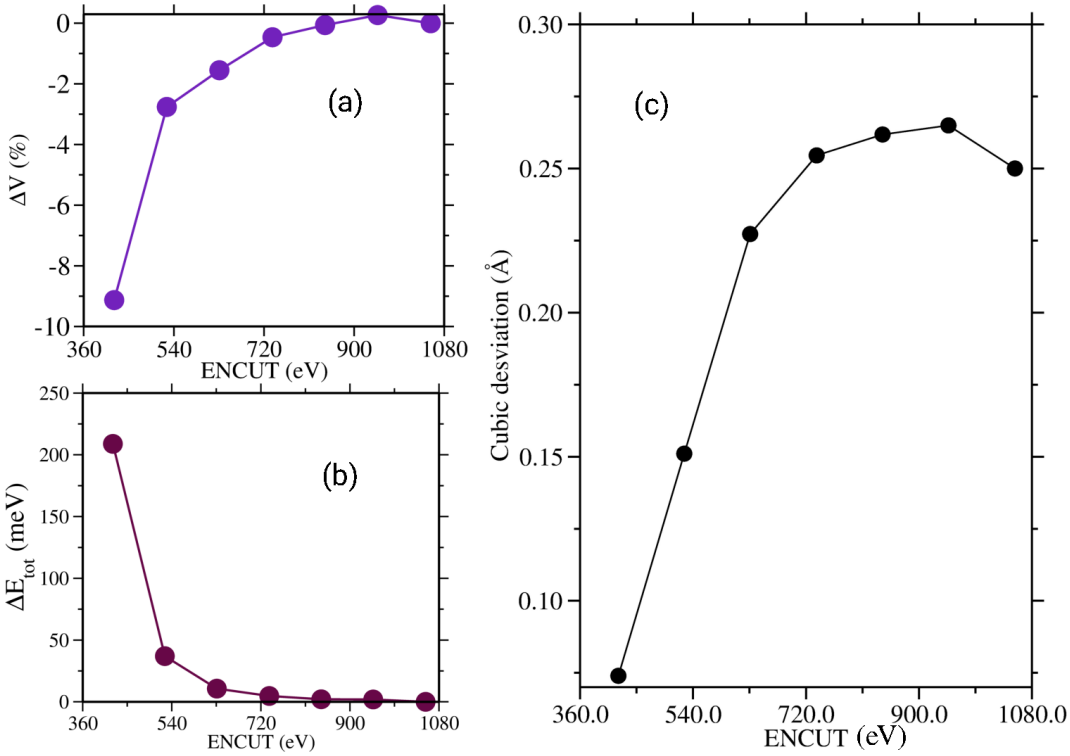

Figure S4 Cubic deviation, relative volume, and relative total energy as a function of cutoff energy.

4 Lowest Energy ASnI$_3$ Perovskites

Table S7 Structural parameters of the lowest energy of ASnI$_3$ perovskites: average ($d^{N/P}_{\mathrm{I-H}}$) and standard deviation ($\sigma^{N/P}_{\mathrm{I-H}}$) of stronger hydrogen bond of $-\mathrm{NH}_x{}^+/-\mathrm{PH}_3{}^+$ group, average ($d^{C}_{\mathrm{I-H}}$) and standard deviation ($\sigma^{C}_{\mathrm{I-H}}$) of stronger hydrogen bond of $-\mathrm{CH}_3$ group, difference of the average hydrogen bonds of $-\mathrm{NH}_x{}^+/-\mathrm{PH}_3{}^+$ and $-\mathrm{CH}_3$ ($\Delta d_{\mathrm{I-H}}$), octahedra effective coordination number (ECN^{Sn}), average ($d^{\mathrm{Sn-I}}_{av}$) and standard deviation of Sn−I bond lengths ($\sigma^{\mathrm{Sn-I}}$), octahedra diagonal I−Sn−I angle (Θ) and standard deviation (σ^{Θ}), octahedra adjacent I−Sn−I angle (θ) and standard deviation (σ^{θ}), distortion index (DI), and bond angle variance (BAV).

	Fase	$d^{N/P}_{\mathrm{I-H}}$ (Å)	$\sigma^{N/P}_{\mathrm{I-H}}$ (Å)	$d^{C}_{\mathrm{I-H}}$ (Å)	$\sigma^{C}_{\mathrm{I-H}}$ (Å)	$\Delta d_{\mathrm{I-H}}$ (Å)	NCE^{Sn} (NNN)	σ^{NCE} (NNN)	$d^{\mathrm{Sn-I}}_{av}$ (Å)	$\sigma^{\mathrm{Sn-I}}$ (Å)	Θ (deg.)	σ^{Θ} (deg.)	θ (deg.)	σ^{θ} (deg.)	ID (%)	VAL (deg.)^2
MASnI$_3$	CI	2.71	0.05	3.32	0.04	0.61	5.75	0.00	3.14	0.10	171.05	1.81	89.95	4.74	1.93	22.50
	PC	2.71	0.07	3.52	0.40	0.81	5.70	0.00	3.14	0.12	170.75	2.66	89.93	4.97	2.37	24.67
	ORC	2.61	0.05	3.12	0.03	0.51	6.00	0.00	3.16	0.01	180.00	0.00	90.00	2.46	0.21	6.03
	TETR	2.65	0.03	3.18	0.10	0.54	6.00	0.00	3.16	0.01	180.00	0.00	90.00	2.61	0.24	6.79
	PH	2.73	0.15	3.24	0.07	0.51	5.89	0.08	3.20	0.07	176.81	1.79	89.99	3.38	1.49	11.95
MPSnI$_3$	CI	2.93	0.33	3.12	0.27	0.19	5.62	0.00	3.17	0.13	174.75	2.75	89.94	2.98	3.33	8.90
	PC	2.94	0.33	3.13	0.28	0.19	5.53	0.00	3.18	0.15	174.68	4.71	89.91	3.43	2.97	11.79
	ORC	3.02	0.08	3.20	0.04	0.18	5.76	0.08	3.17	0.10	175.13	2.18	89.95	3.79	2.59	15.36
	TETR	3.05	0.02	3.09	0.02	0.04	6.00	0.00	3.16	0.06	180.00	0.00	90.00	1.40	0.33	1.97
	PH	2.89	0.20	3.17	0.23	0.28	5.91	0.04	3.20	0.06	176.84	1.02	90.07	2.91	1.75	9.06
FASnI$_3$	CI	2.78	0.22	3.28	0.00	0.50	5.49	0.00	3.18	0.15	171.13	1.52	90.00	4.67	3.97	21.85
	PC	2.81	0.24	3.22	0.00	0.41	5.21	0.00	3.19	0.21	169.93	2.98	89.93	5.41	4.34	29.27
	ORC	2.77	0.06	3.11	0.00	0.35	5.22	0.00	3.19	0.20	171.63	6.95	89.85	6.94	4.90	48.19
	TETR	3.23	0.27	3.22	0.00	−0.01	5.97	0.00	3.14	0.04	176.69	2.88	90.04	2.12	0.98	4.50
	PH	2.88	0.11	3.15	0.01	0.27	5.73	0.19	3.20	0.11	175.72	2.60	90.00	4.99	2.88	26.07

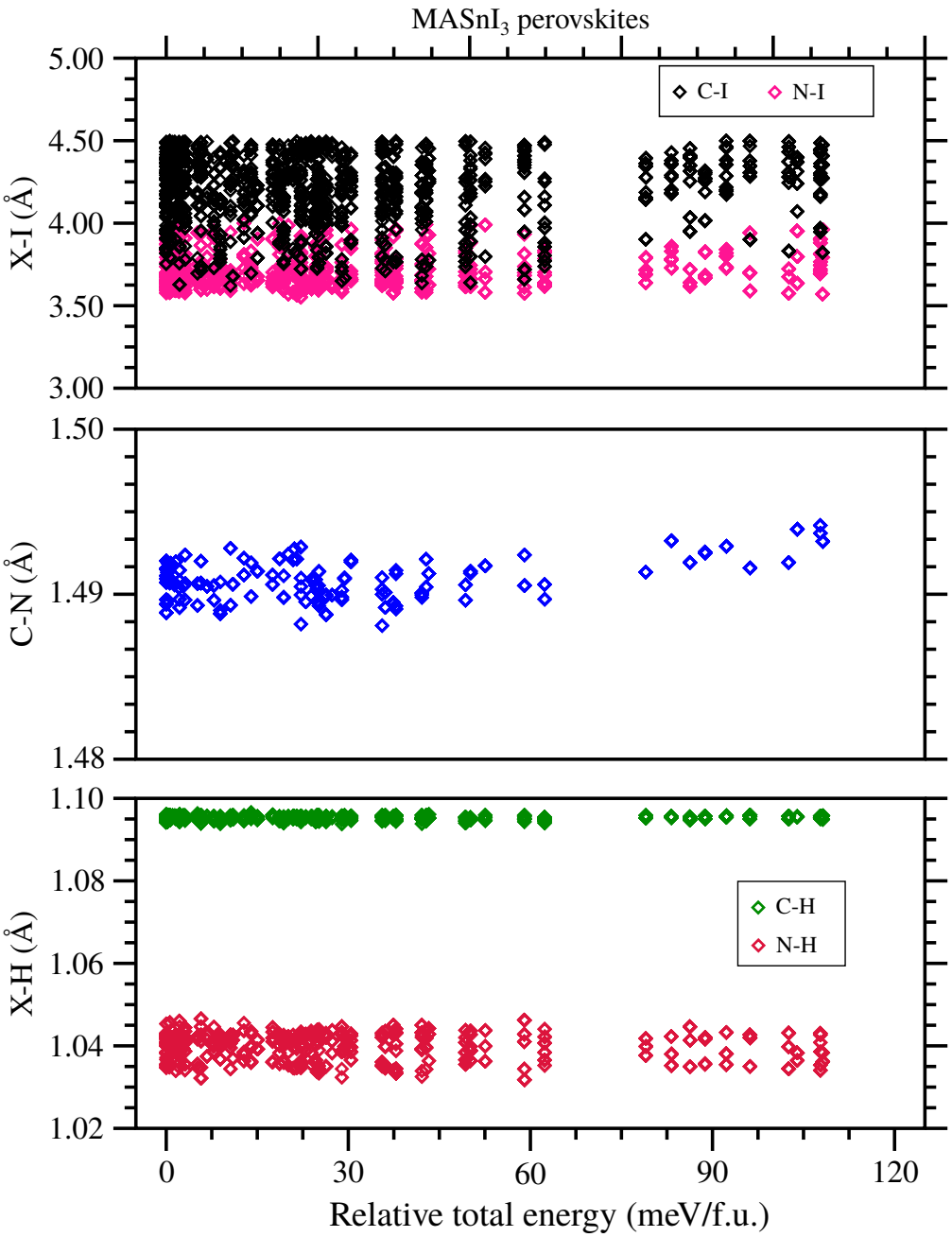

Figure S5 $MASnI_3$ perovskites: X−H and C−N bond lengths of *A*-cation, and distance from C/N to iodide of inorganic-framework.

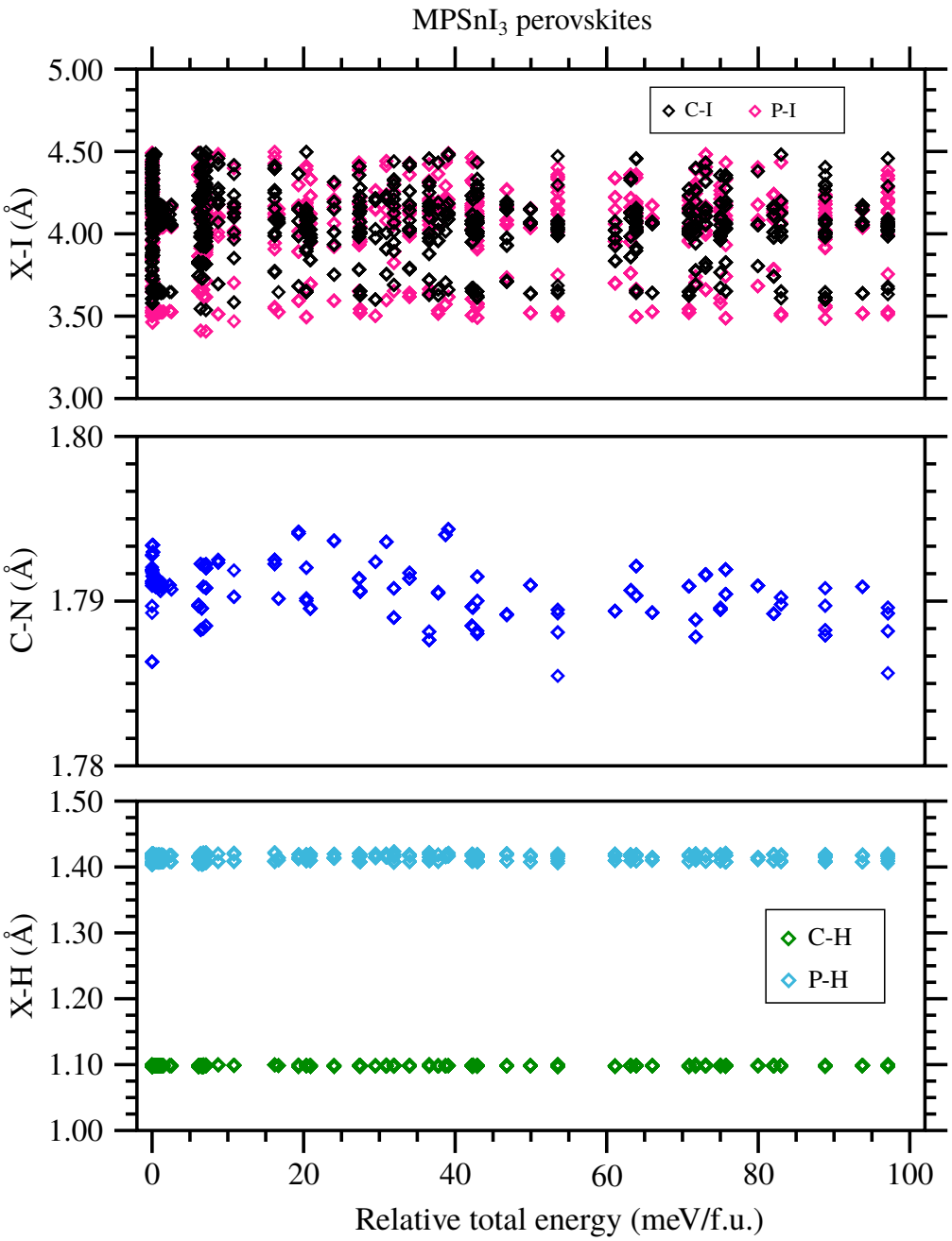

Figure S6 MPSnI$_3$ perovskites: X−H and C−P bond lengths of *A*-cation, and distance from C/P to iodide of inorganic-framework.

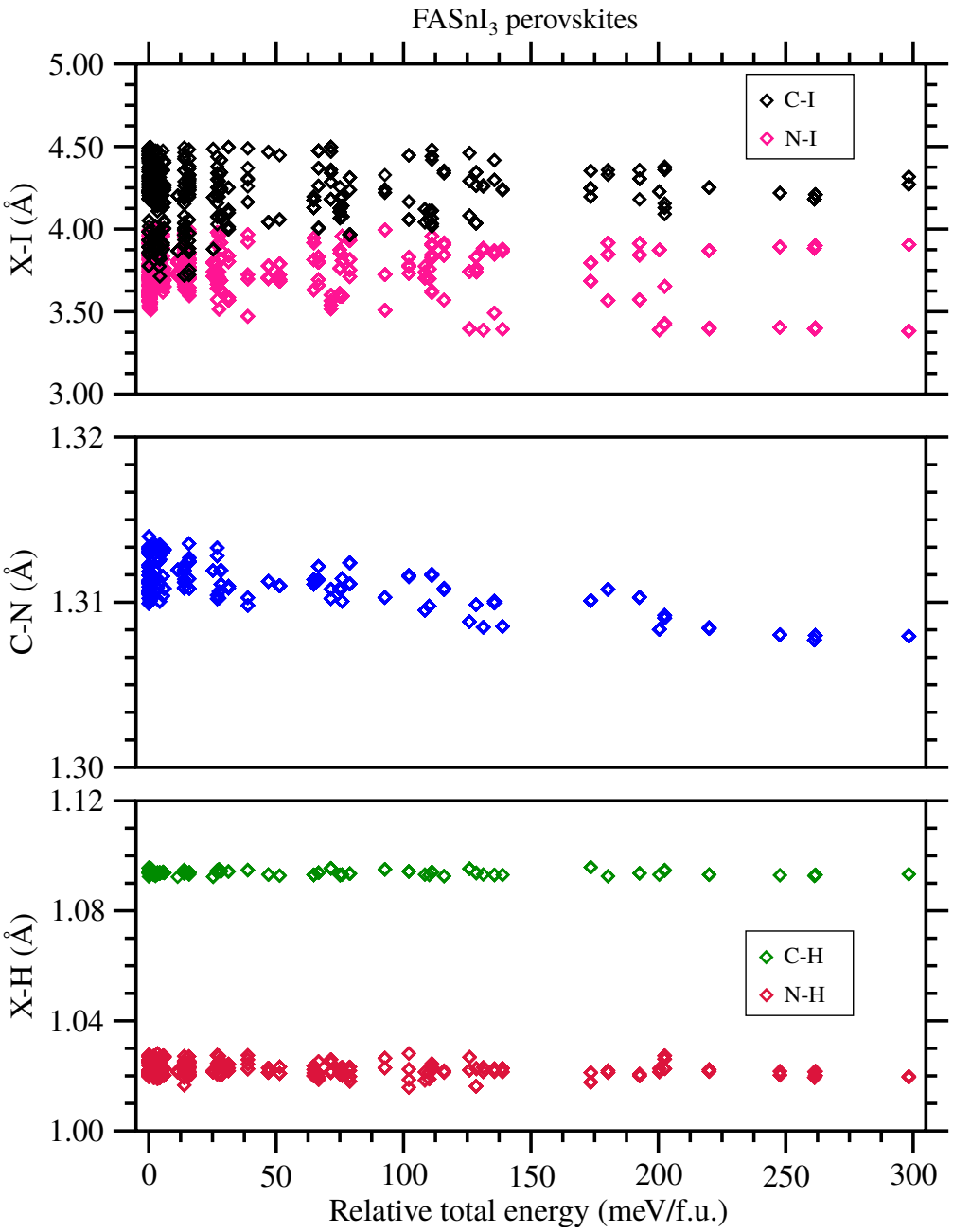

Figure S7 $FASnI_3$ perovskites: X−H and C−N bond lengths of *A*-cation, and distance from C/N to iodide of inorganic-framework.

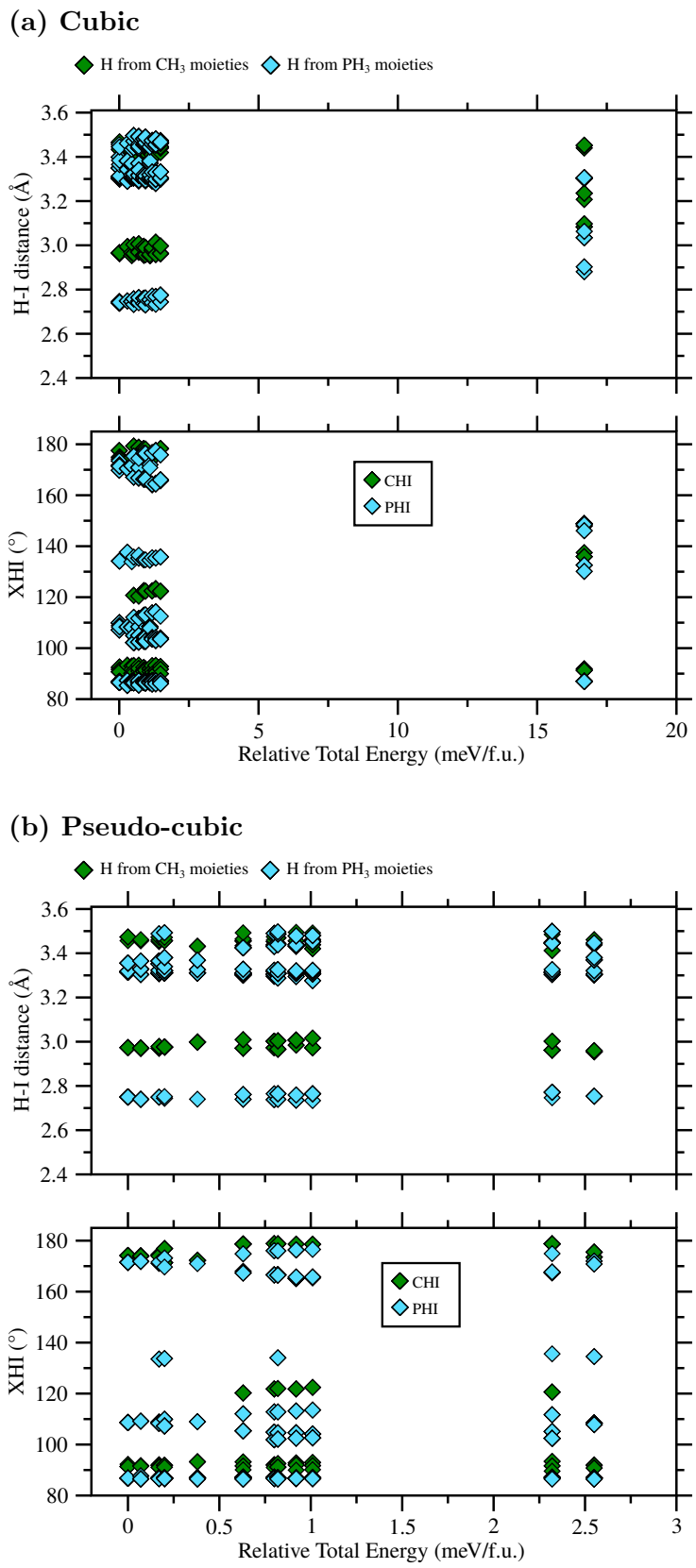

Figure S8 Relative energy versus all H···I distances and angles (CHI and PHI) of cubic and pseudo-cubic $MPSnI_3$ perovskites in a cutoff radius of 3.5 Å.

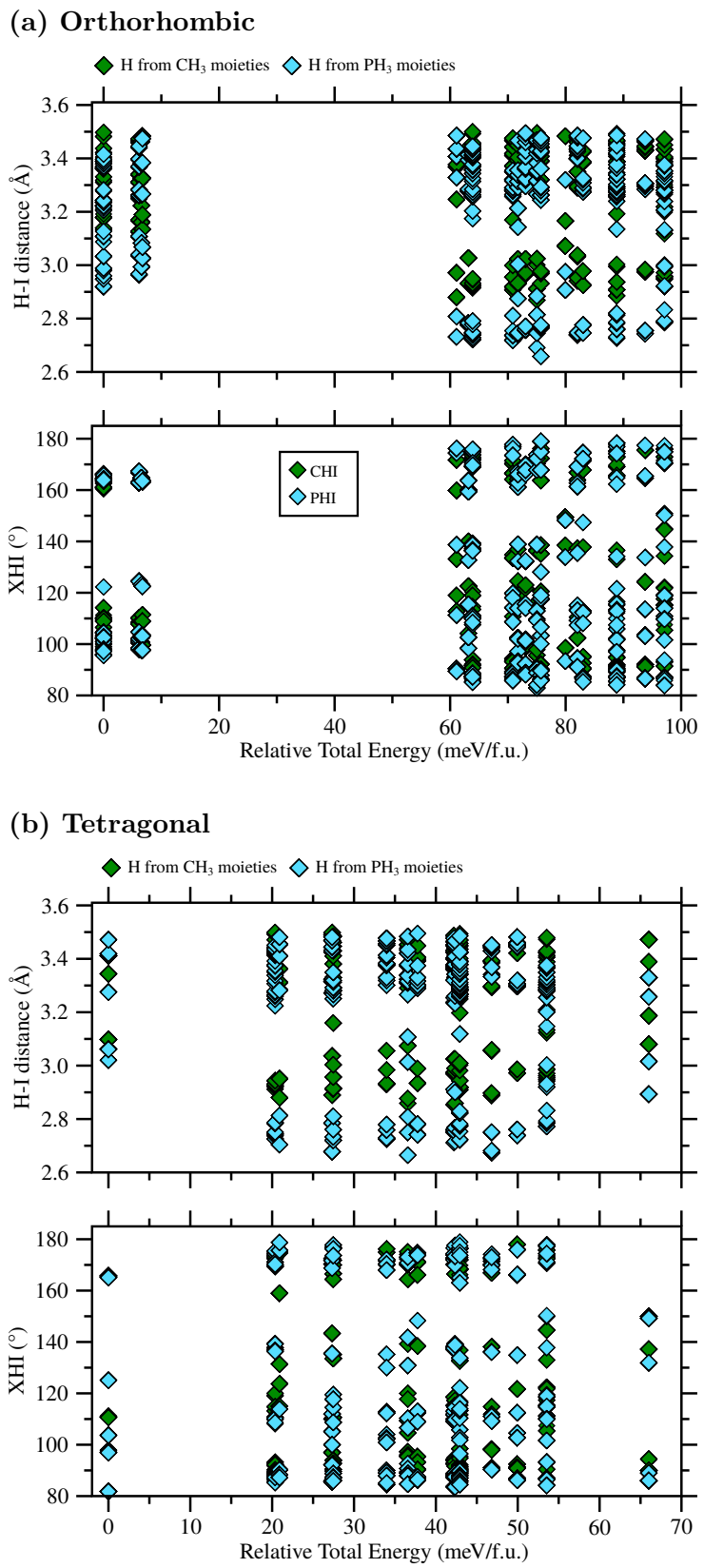

Figure S9 Relative energy versus all H···I distances and angles (CHI and PHI) of orthorhombic and tetragonal $MPSnI_3$ perovskites in a cutoff radius of 3.5 Å.

(a) Hexagonal

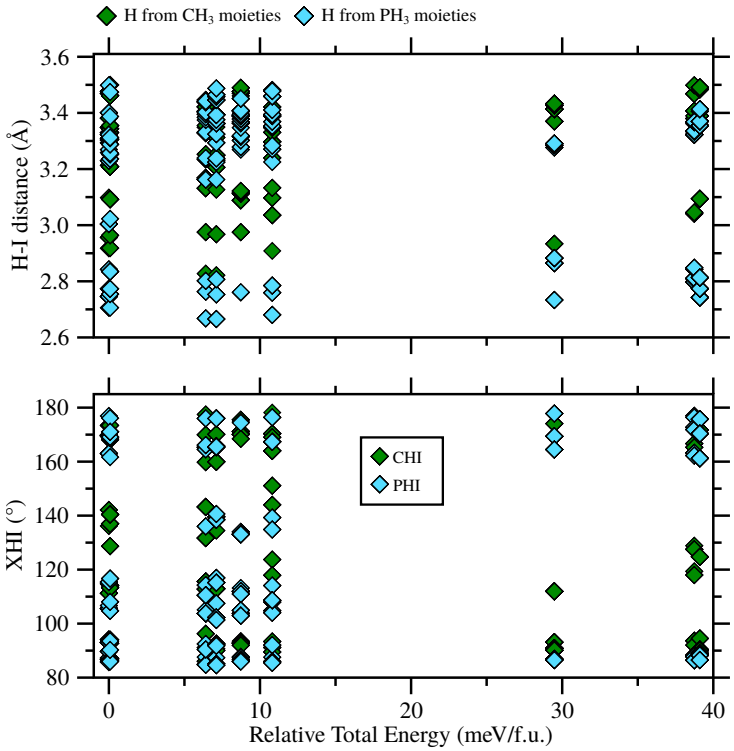

(b) Pseudo-hexagonal

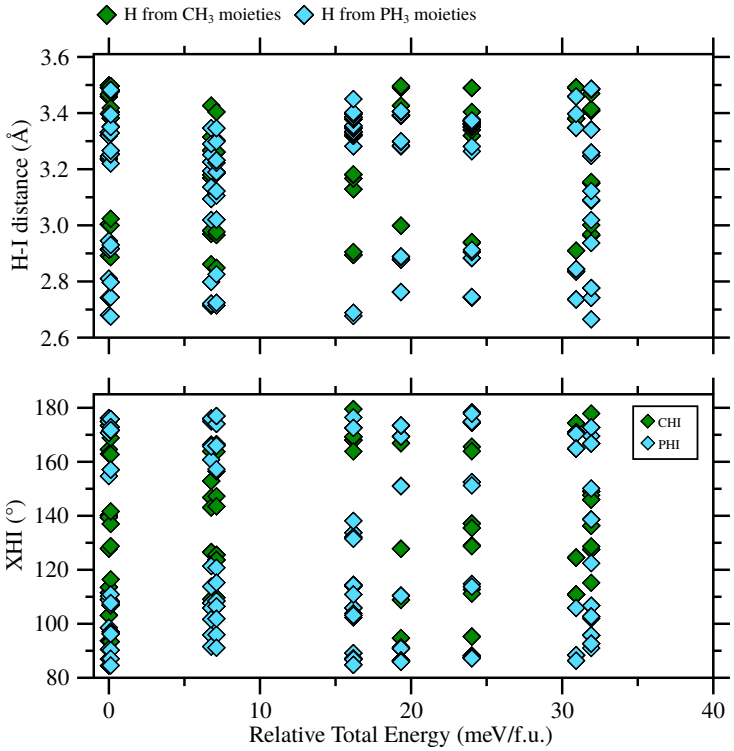

Figure S10 Relative energy versus all H···I distances and angles (CHI and PHI) of hexagonal and pseudo-hexagonal $MPSnI_3$ perovskites in a cutoff radius of 3.5 Å.

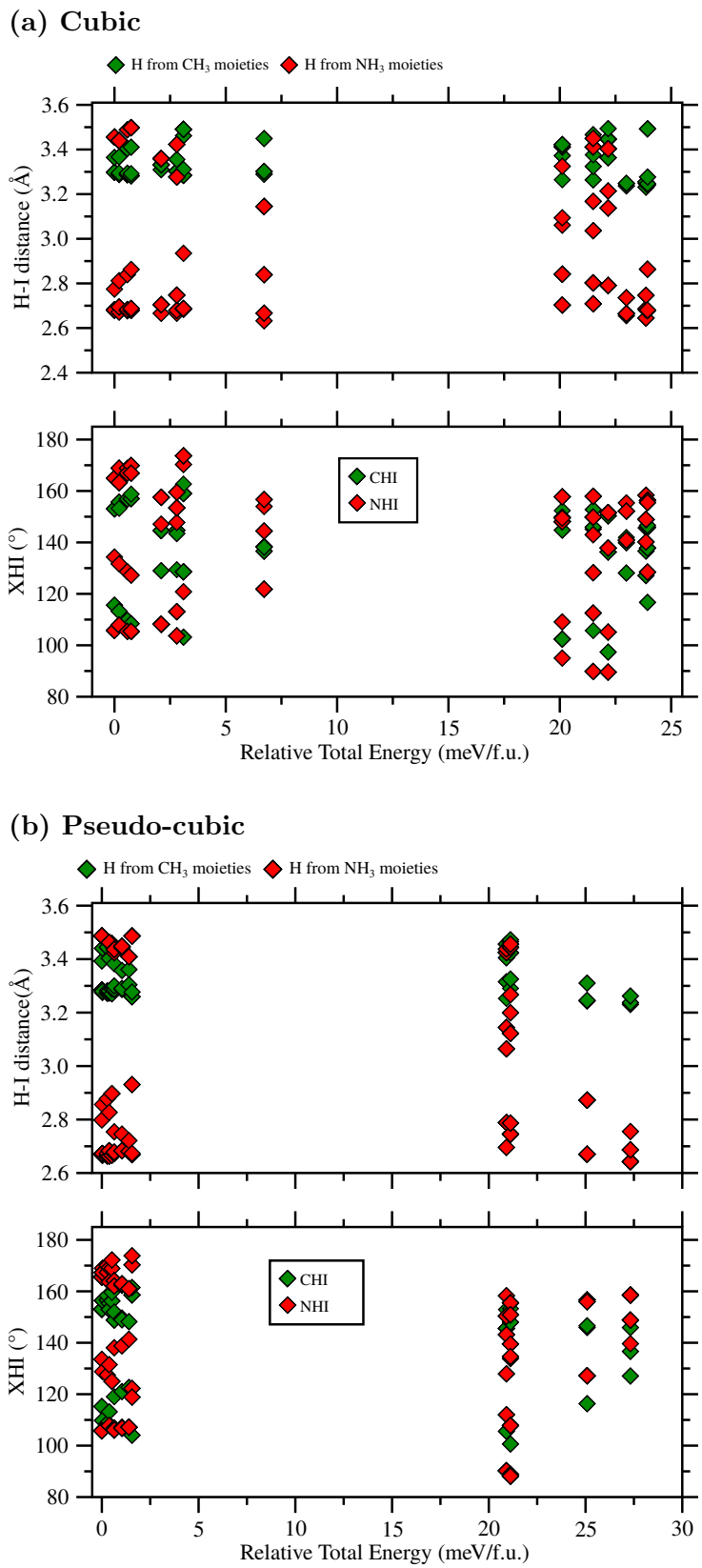

Figure S11 Relative energy versus all H···I distances and angles (CHI and NHI) of cubic and pseudo-cubic $MASnI_3$ perovskites in a cutoff radius of 3.5 Å.

(a) Orthorhombic

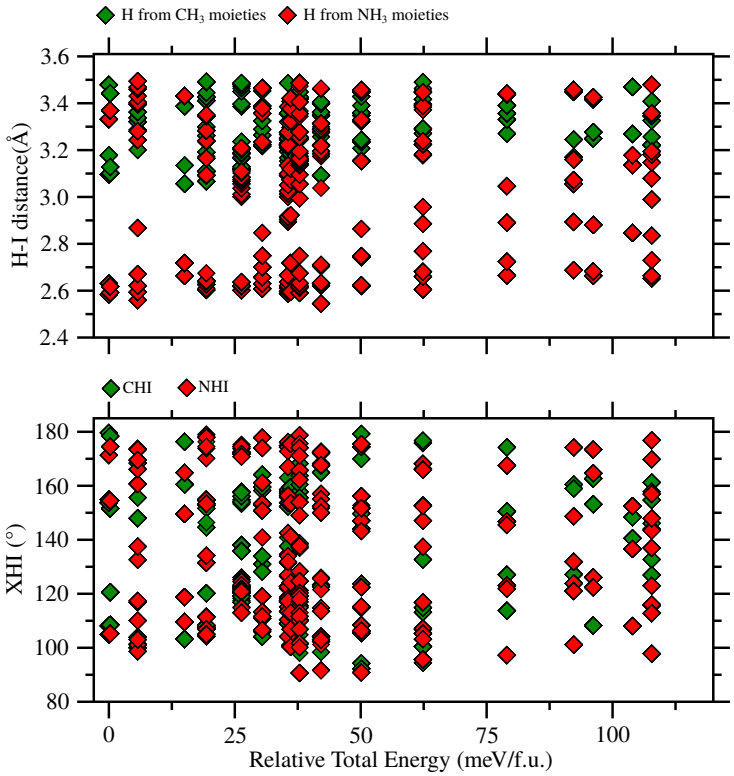

(b) Tetragonal

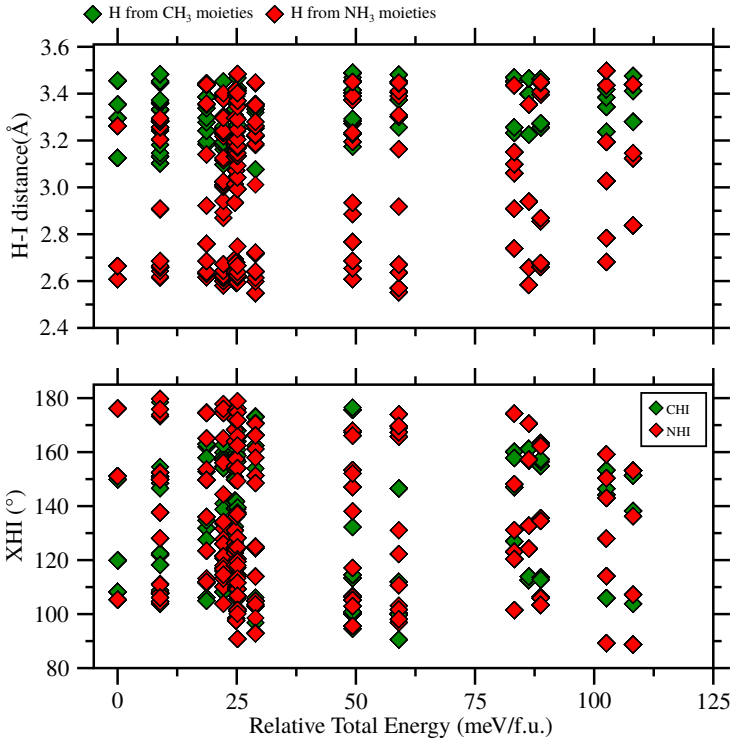

Figure S12 Relative energy versus all H···I distances and angles (CHI and NHI) of orthorhombic and tetragonal $MASnI_3$ perovskites in a cutoff radius of 3.5 Å.

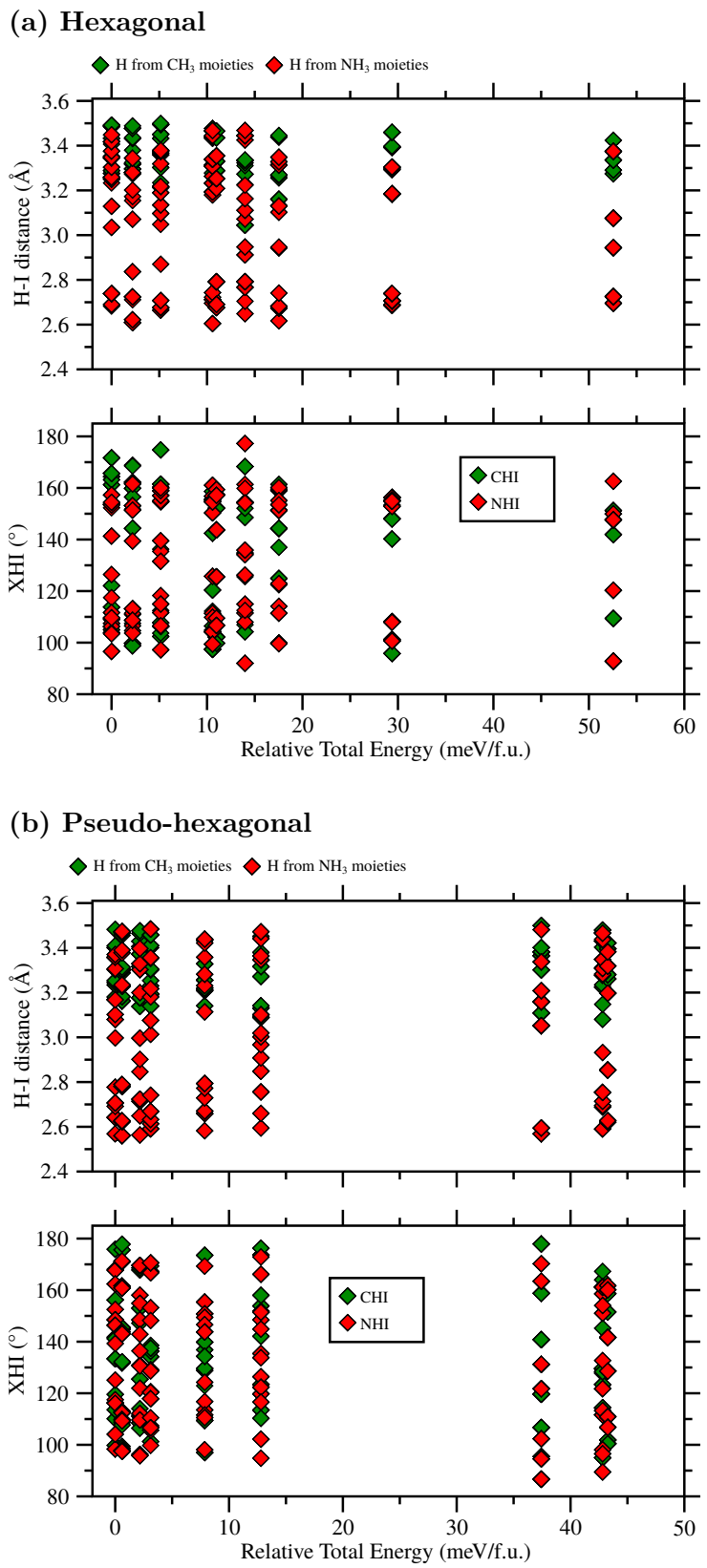

Figure S13 Relative energy versus all H···I distances and angles (CHI and NHI) of hexagonal and pseudo-hexagonal $MASnI_3$ perovskites in a cutoff radius of 3.5 Å.

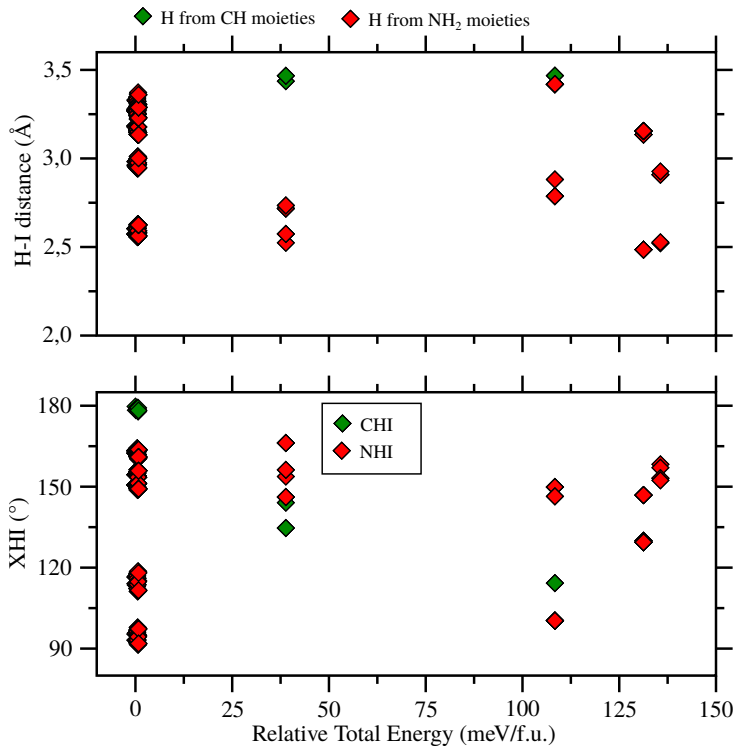

(a) Cubic

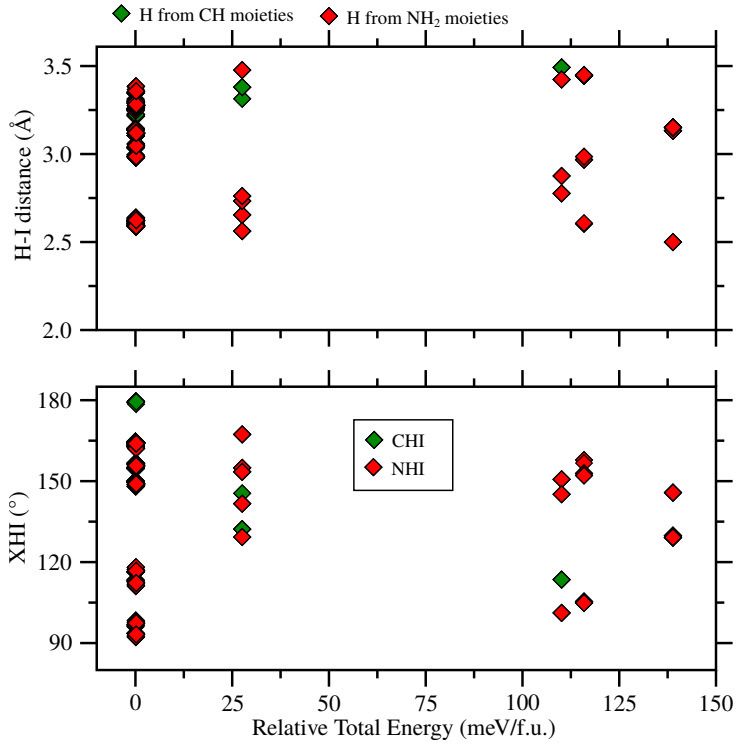

(b) Pseudo-cubic

Figure S14 Relative energy versus all H···I distances and angles (CHI and NHI) of cubic and pseudo-cubic $FASnI_3$ perovskites in a cutoff radius of 3.5 Å.

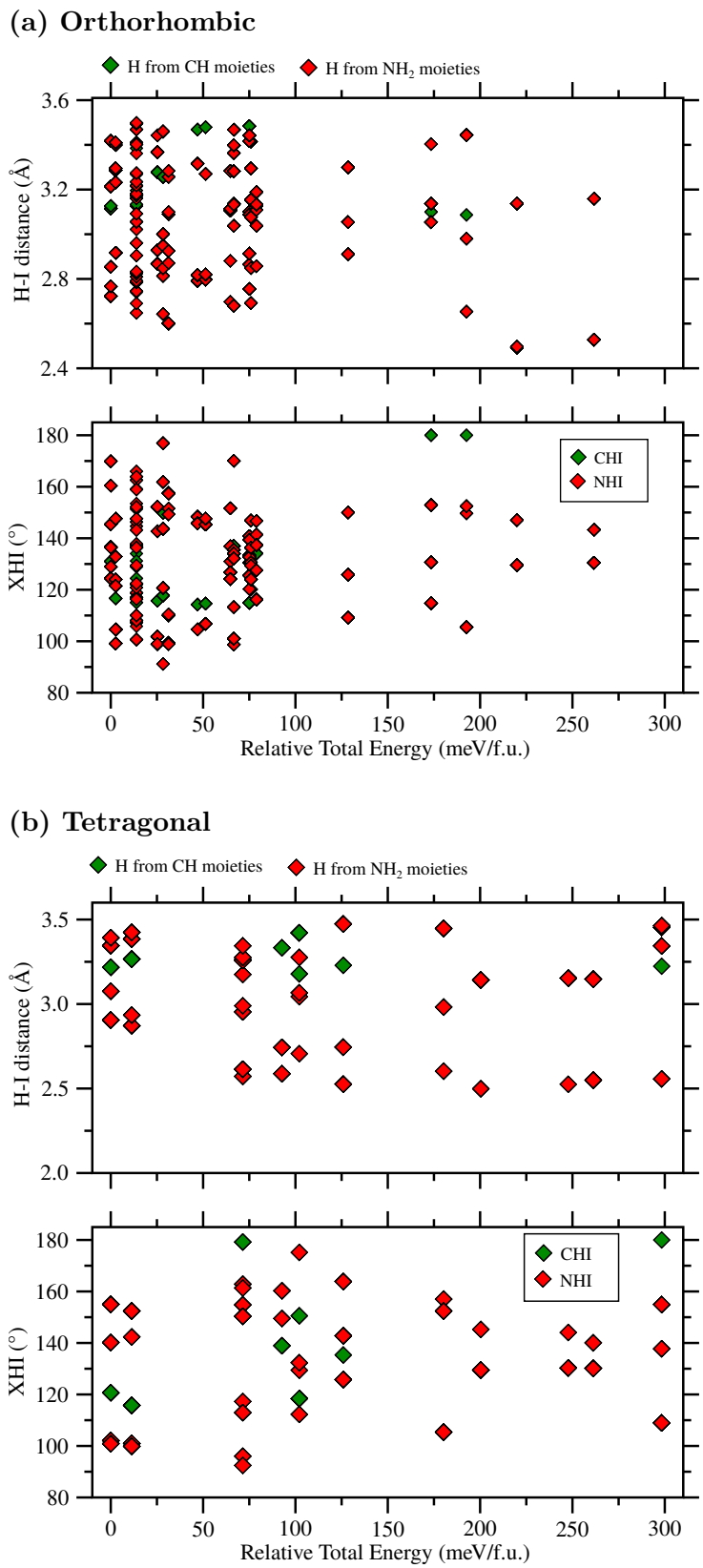

Figure S15 Relative energy versus all H···I distances and angles (CHI and NHI) of orthorhombic and tetragonal $FASnI_3$ perovskites in a cutoff radius of 3.5 Å.

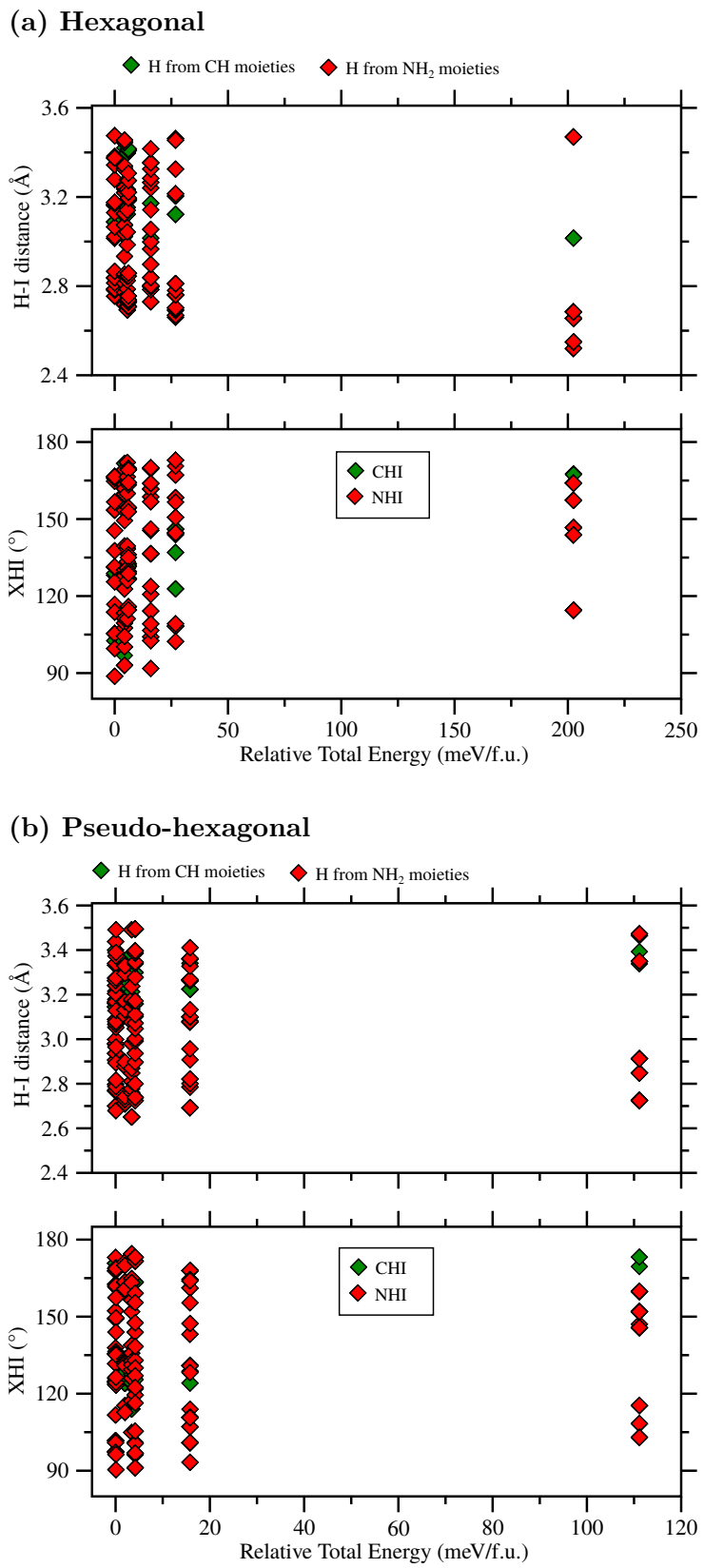

Figure S16 Relative energy versus all H···I distances and angles (CHI and NHI) of hexagonal and pseudo-hexagonal $FASnI_3$ perovskites in a cutoff radius of 3.5 Å.

(a) Cubic

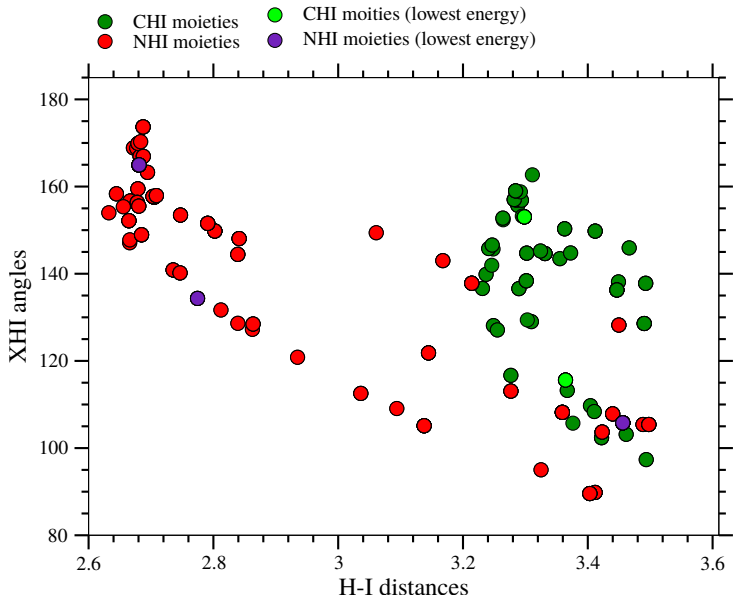

(b) Pseudo-cubic

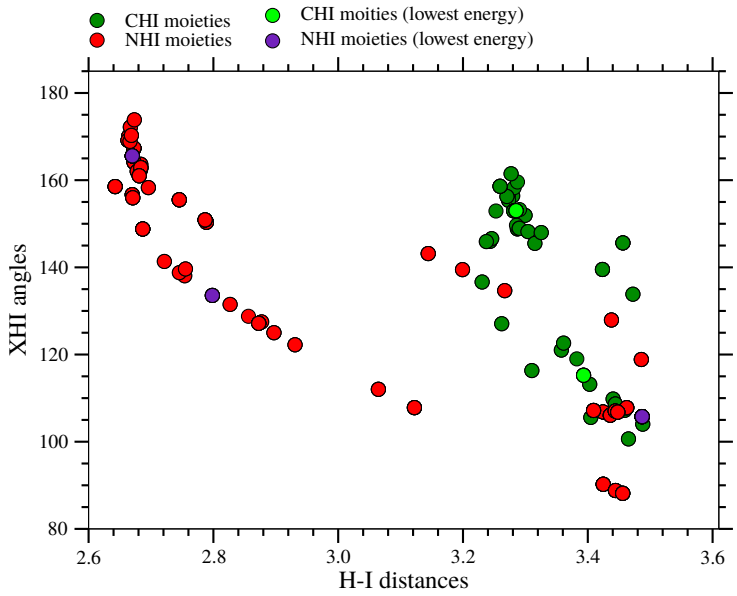

Figure S17 All CHI and NHI angles of the cubic and pseudo-cubic $MASnI_3$ perovskites in a cutoff radius of 3.5 Å versus the H···I distances. The values of the lowest energy cubic perovskite are highlighted in the plot.

(a) Orthorhombic

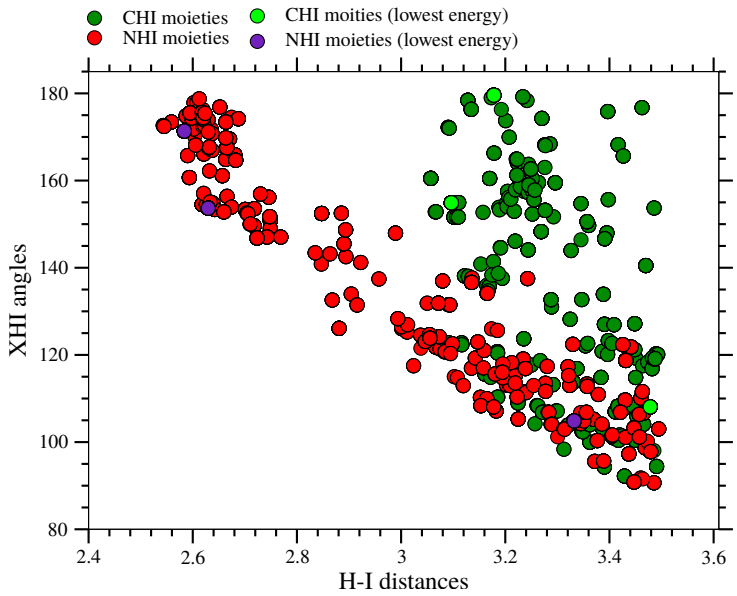

(b) Tetragonal

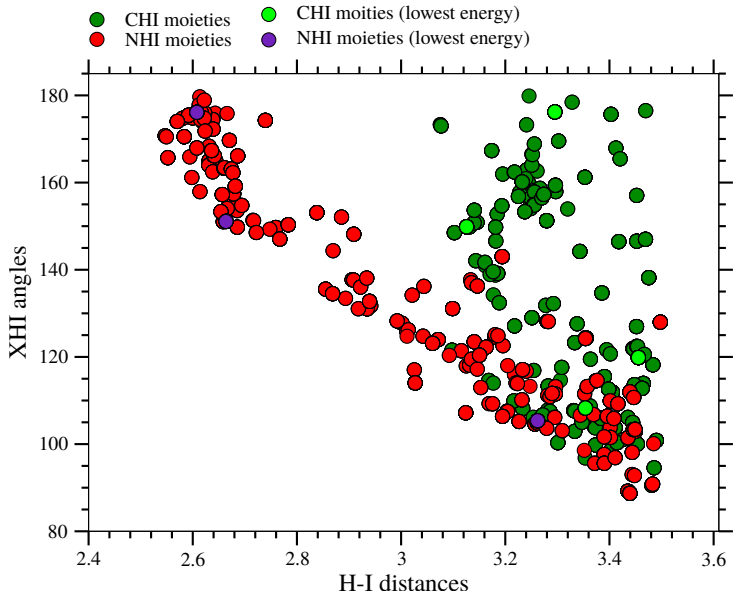

Figure S18 All CHI and NHI angles of the orthorhombic and tetragonal $MASnI_3$ perovskites in a cutoff radius of 3.5 Å versus the H···I distances. The values of the lowest energy cubic perovskite are highlighted in the plot.

(a) Hexagonal

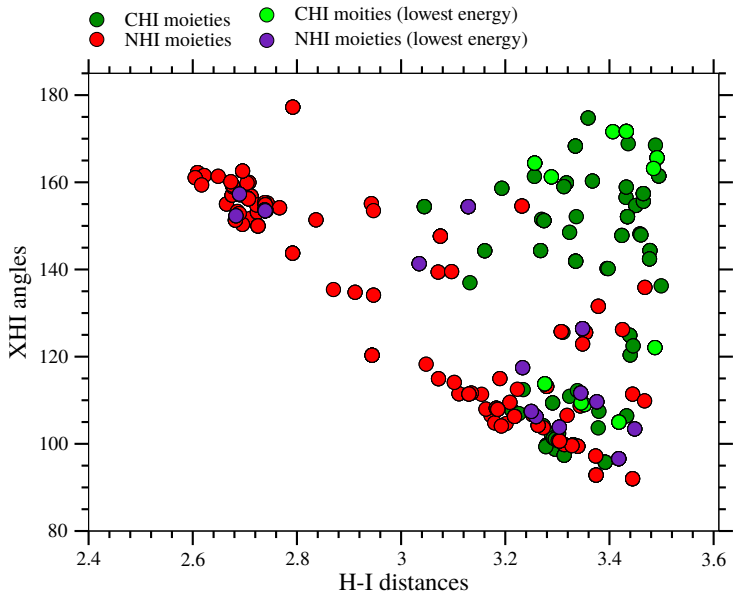

(b) Pseudo-hexagonal

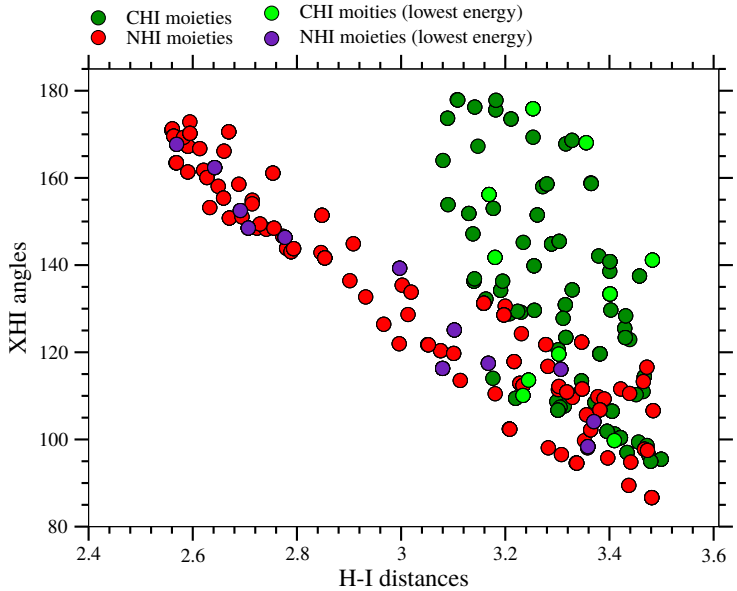

Figure S19 All CHI and NHI angles of the hexagonal and pseudo-hexagonal $MASnI_3$ perovskites in a cutoff radius of 3.5 Å versus the H···I distances. The values of the lowest energy cubic perovskite are highlighted in the plot.

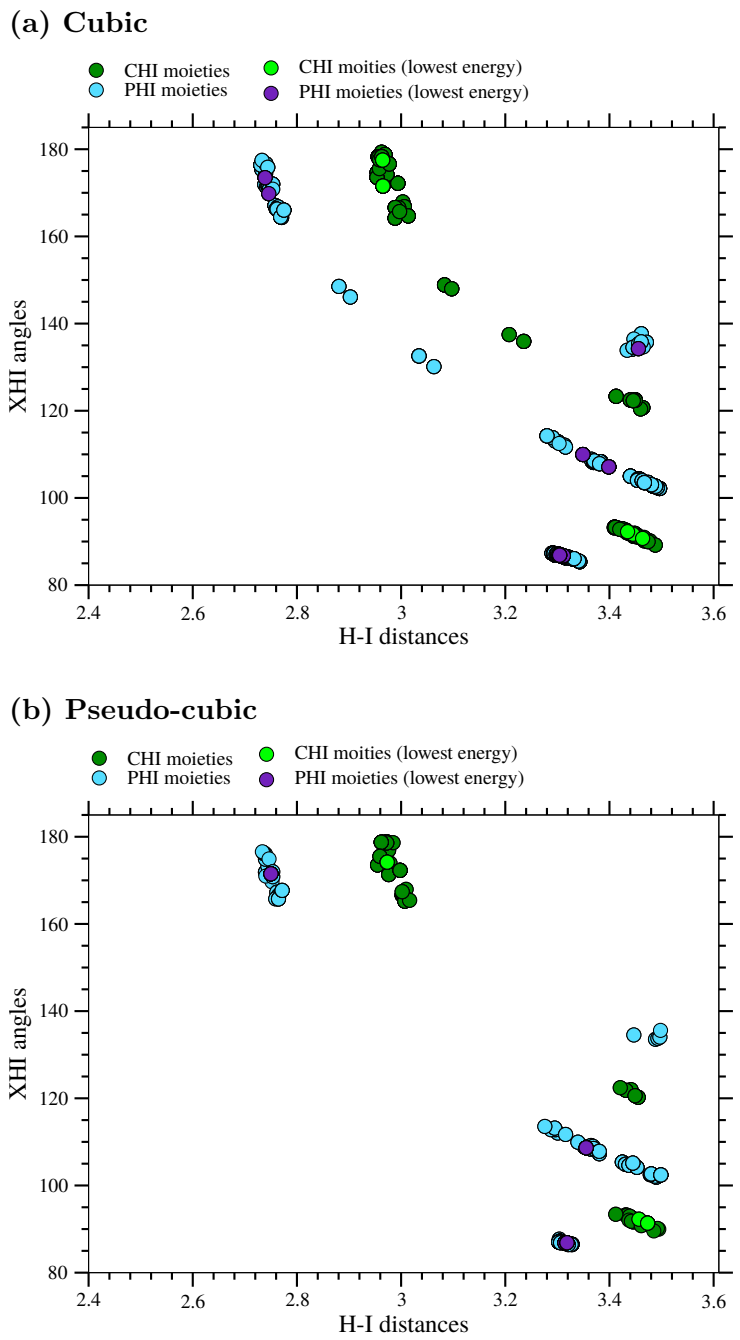

Figure S20 All CHI and PHI angles of the cubic and pseudo-cubic $MPSnI_3$ perovskites in a cutoff radius of 3.5 Å versus the H···I distances. The values of the lowest energy cubic perovskite are highlighted in the plot.

(a) Orthorhombic

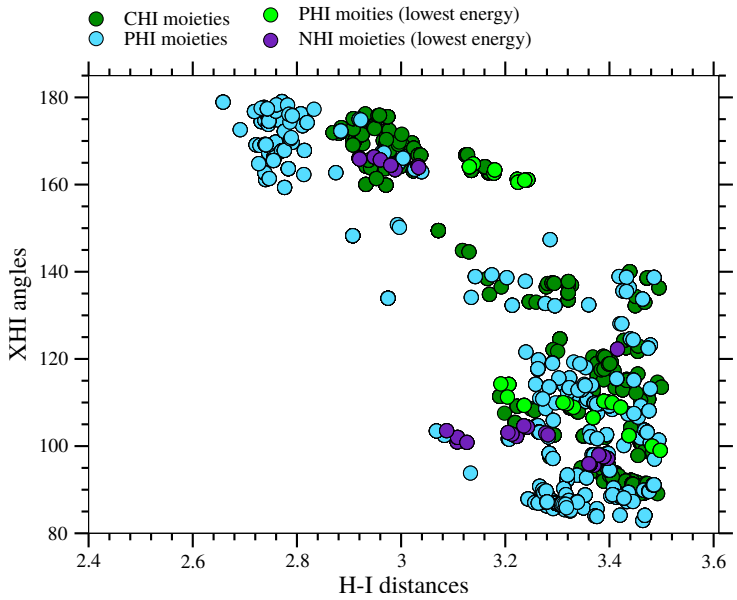

(b) Tetragonal

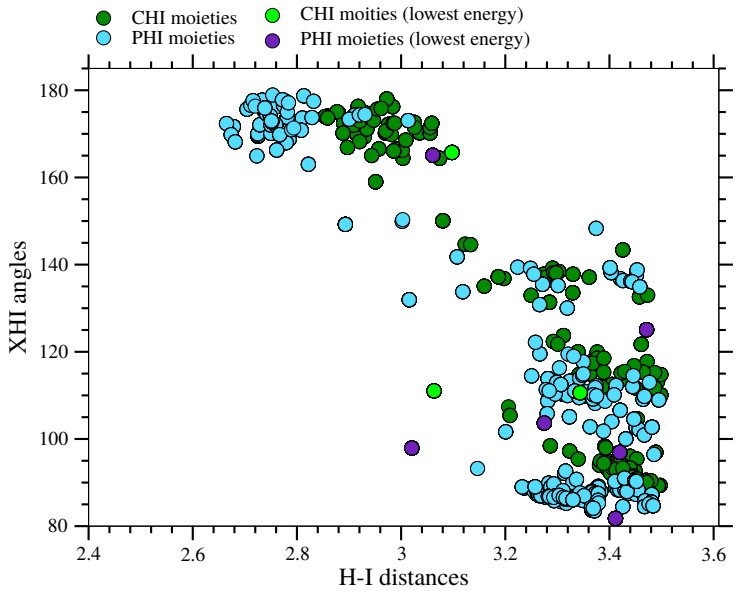

Figure S21 All CHI and PHI angles of the orthorhombic and tetragonal $MPSnI_3$ perovskites in a cutoff radius of 3.5 Å versus the H···I distances. The values of the lowest energy cubic perovskite are highlighted in the plot.

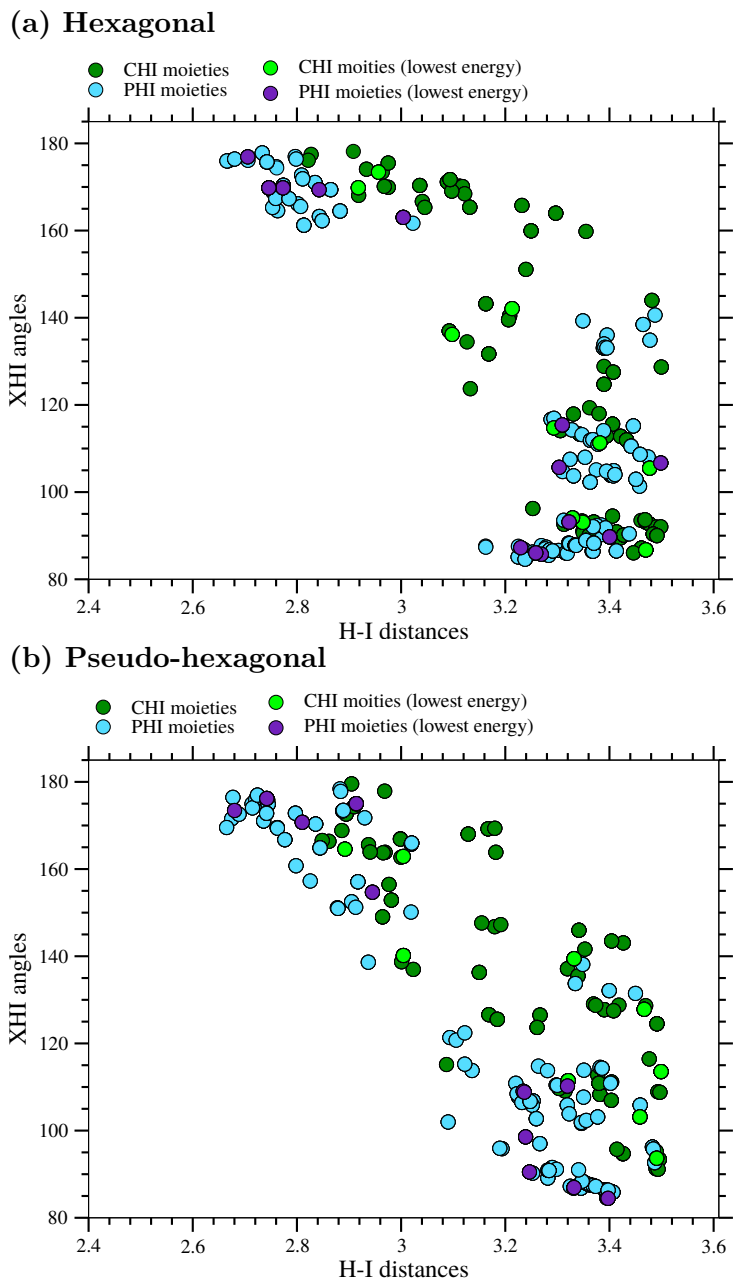

Figure S22 All CHI and PHI angles of the hexagonal and pseudo-hexagonal $MPSnI_3$ perovskites in a cutoff radius of 3.5 Å versus the H···I distances. The values of the lowest energy cubic perovskite are highlighted in the plot.

(a) Cubic

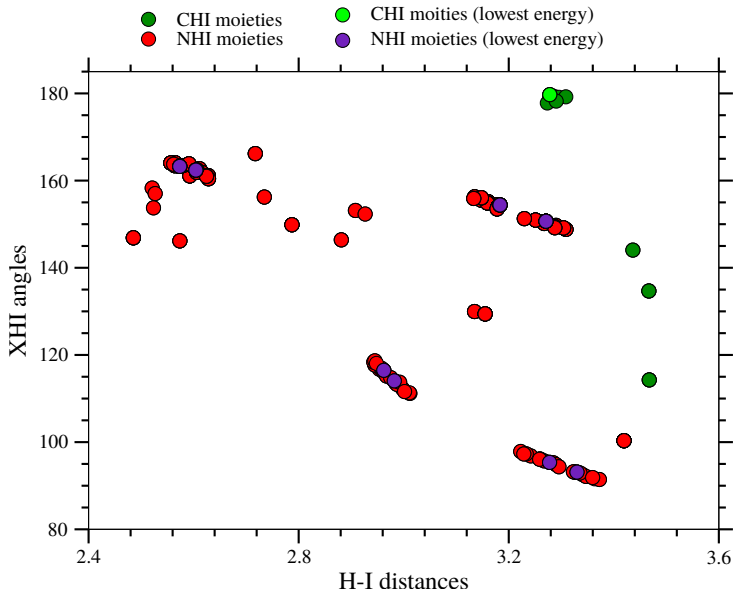

(b) Pseudo-cubic

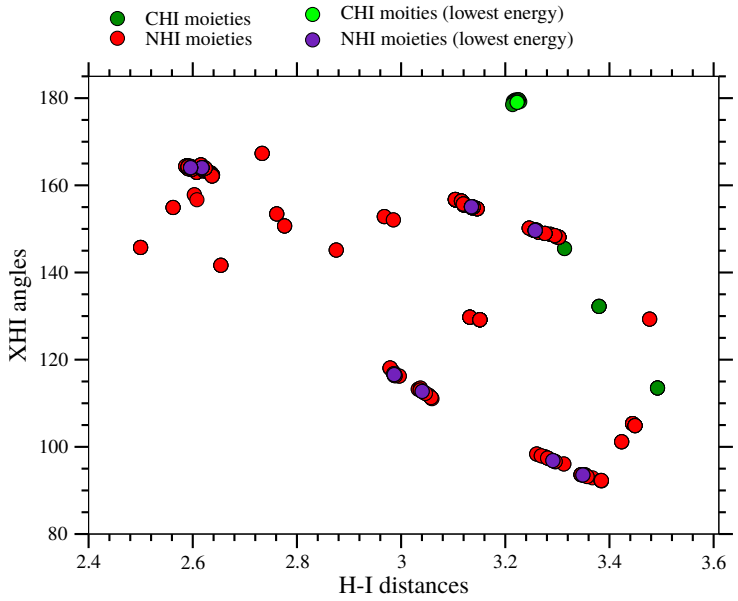

Figure S23 All CHI and NHI angles of the cubic and pseudo-cubic $FASnI_3$ perovskites in a cutoff radius of $3.5\,\text{Å}$ versus the H···I distances. The values of the lowest energy cubic perovskite are highlighted in the plot.

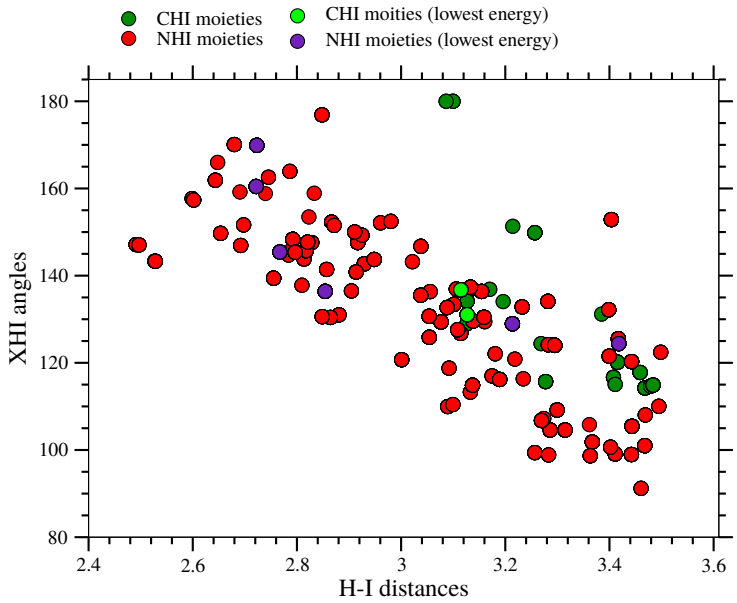

(a) Orthorhombic

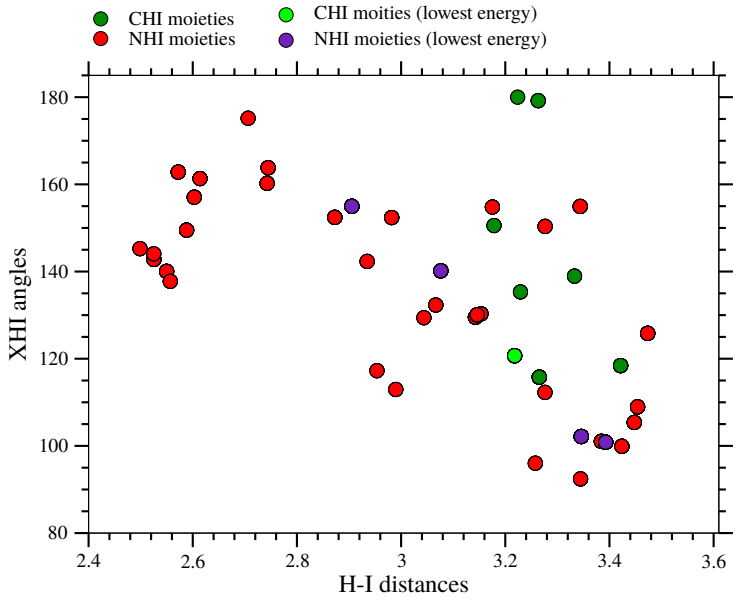

(b) Tetragonal

Figure S24 All CHI and NHI angles of the orthorhombic and tetragonal $FASnI_3$ perovskites in a cutoff radius of 3.5 Å versus the H···I distances. The values of the lowest energy cubic perovskite are highlighted in the plot.

(a) Hexagonal

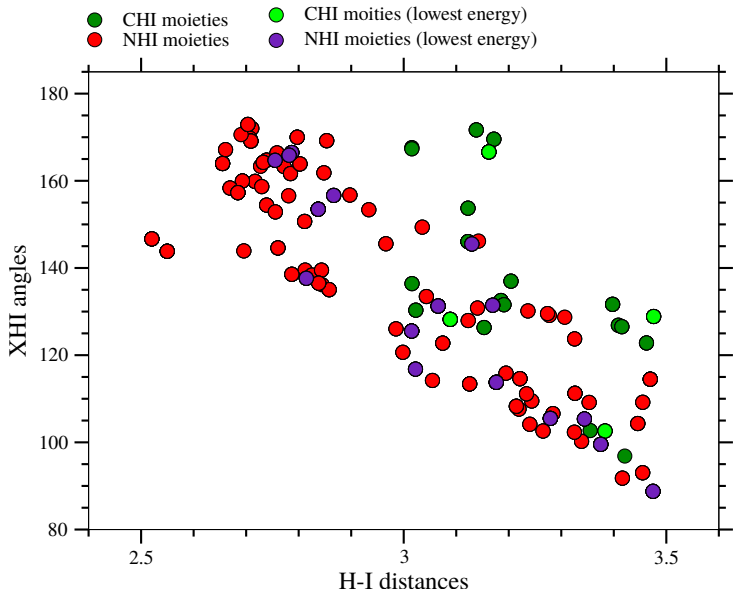

(b) Pseudo-hexagonal

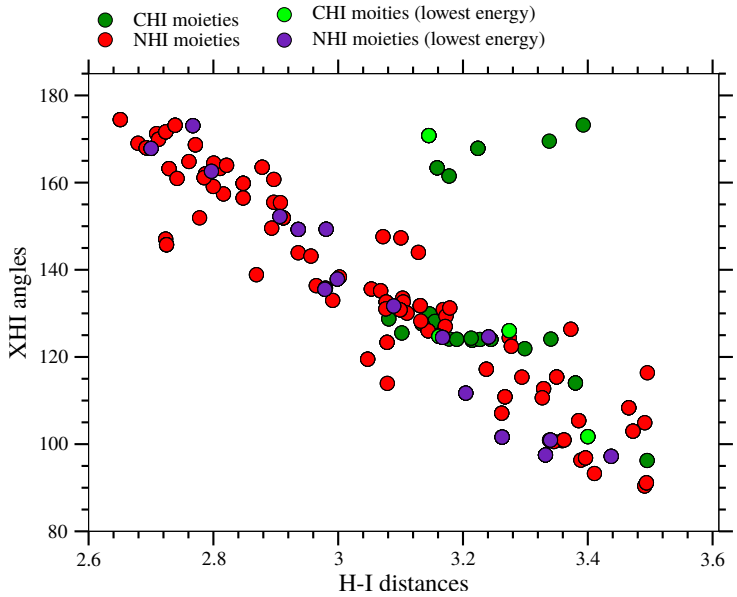

Figure S25 All CHI and NHI angles of the hexagonal and pseudo-hexagonal $FASnI_3$ perovskites in a cutoff radius of 3.5 Å versus the H···I distances. The values of the lowest energy cubic perovskite are highlighted in the plot.

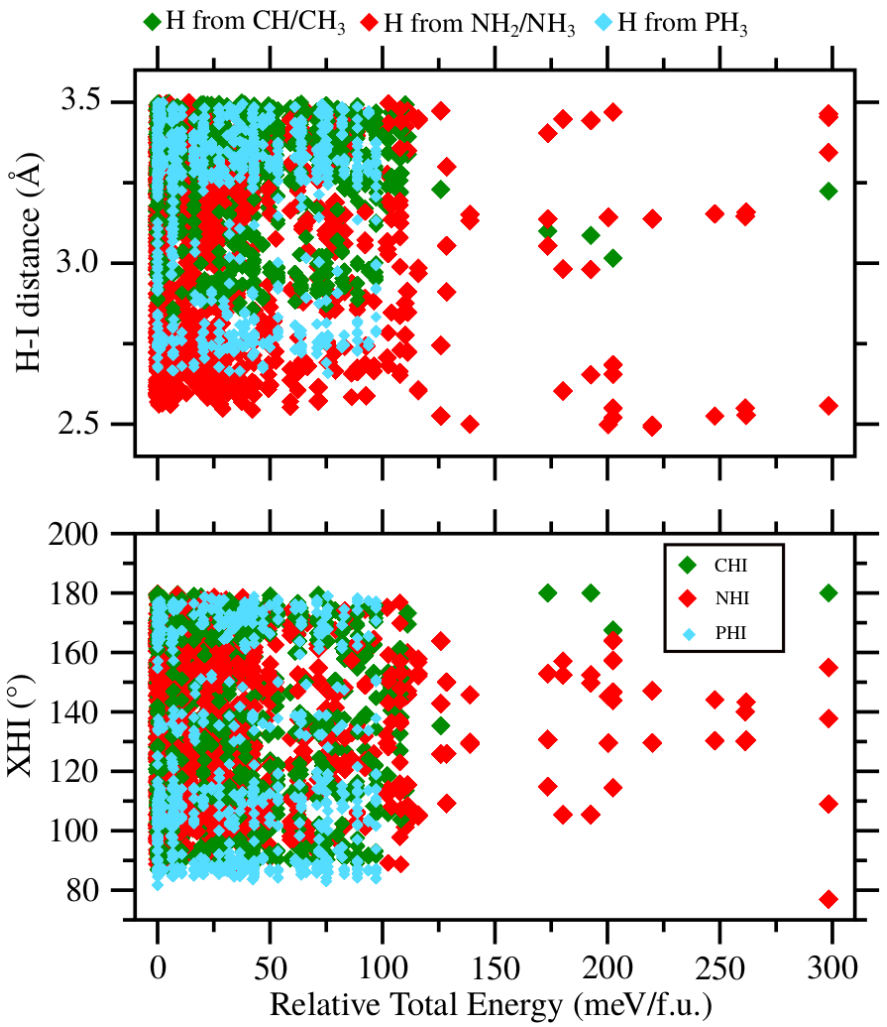

Figure S26 All H···I distances and XHI angles (X = C, N or P) versus the relative total energy of ASnI$_3$ perovskites.

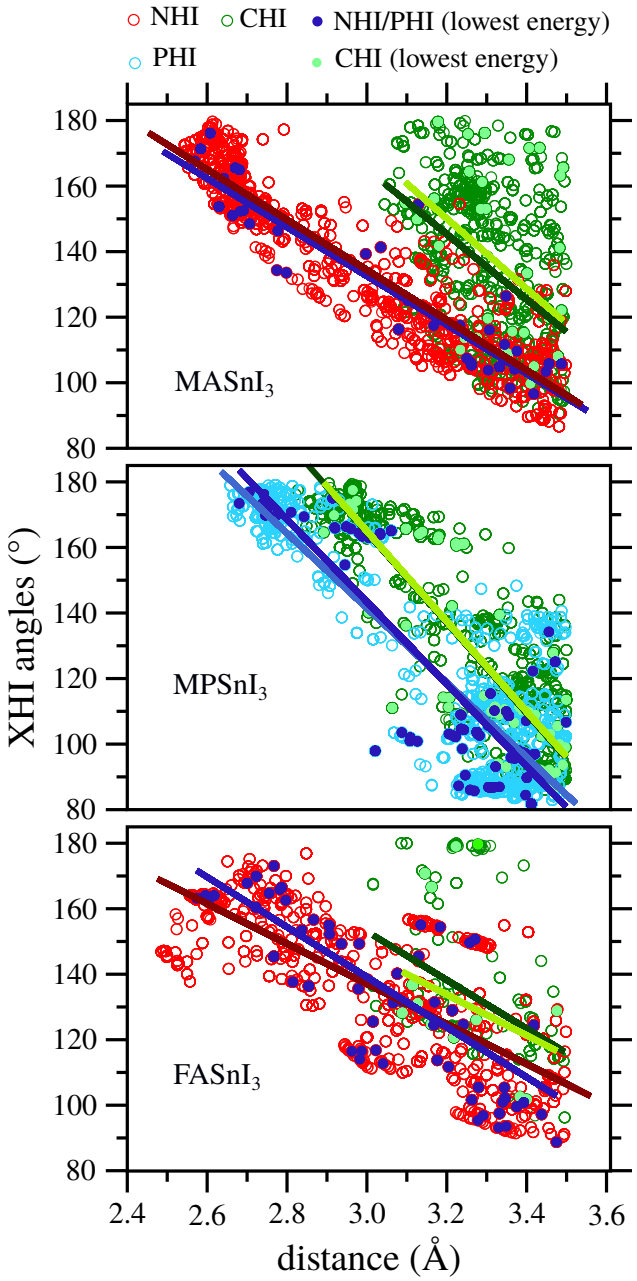

Figure S27 All XHI angles (X = C, N or P) versus the H···I distances for ASnI$_3$ perovskites. The red, dark green and light blue color lines represents the fitting of all data of NHI, CHI and PHI angles versus distance, respectively. The light green and blue curves represent the fitting for the dots of lowest energy perovskites.

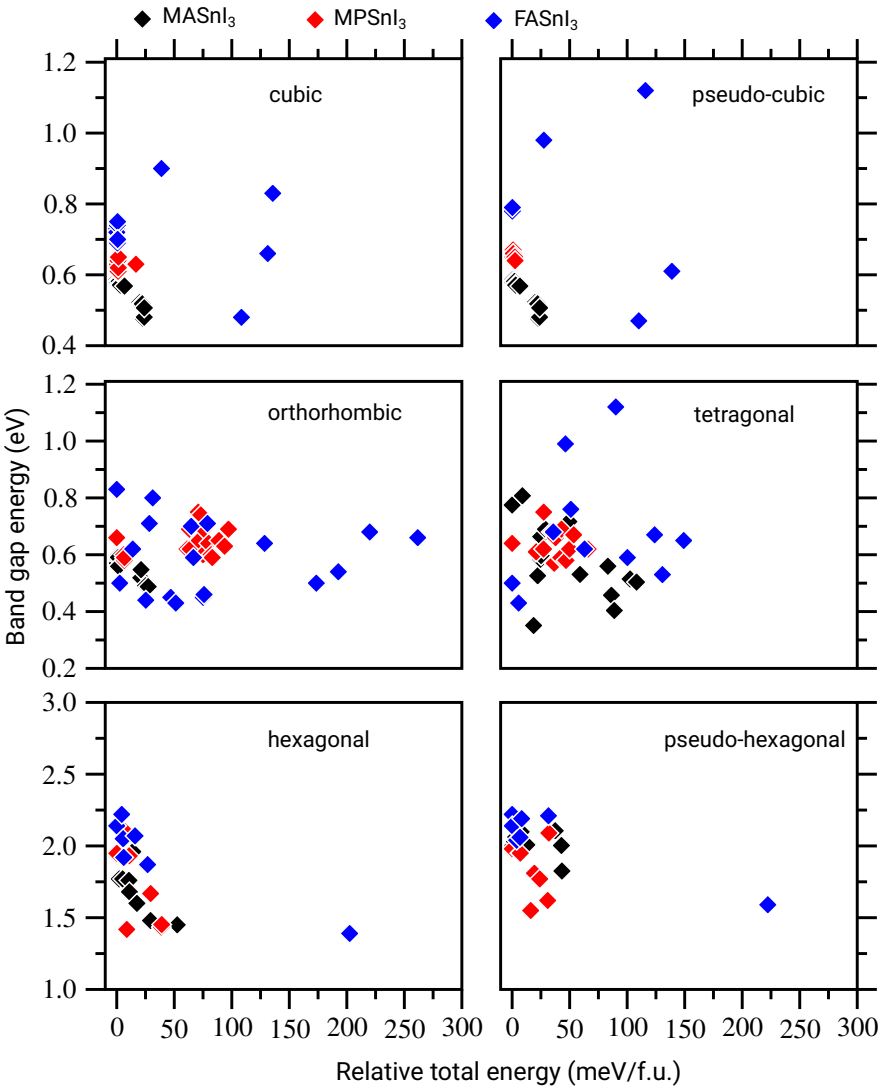

Figure S28 Band gap energy of ASnI$_3$ perovskites as a function of the relative total energy.

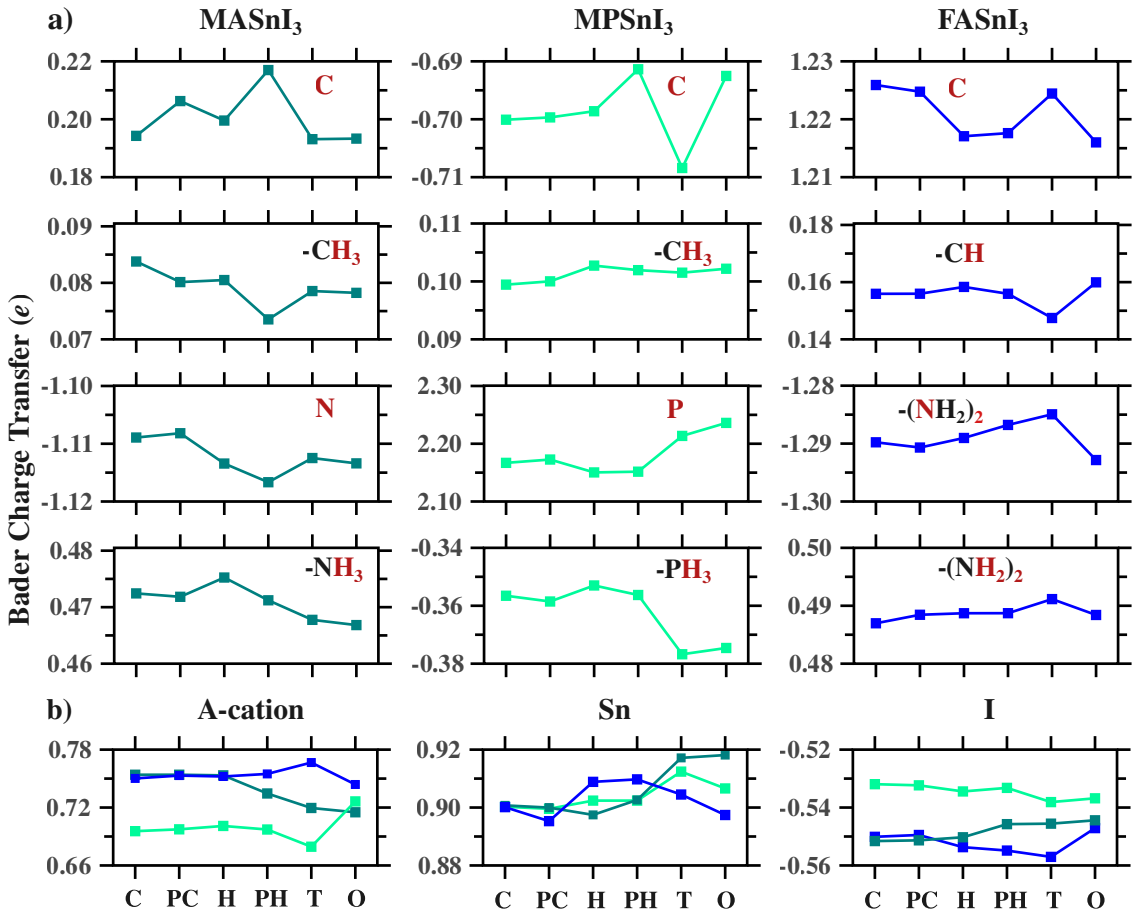

Figure S29 a) Average Bader charge for each element of ASnI$_3$ perovskites. b) Average Bader charge on A-cation, Sn and I.

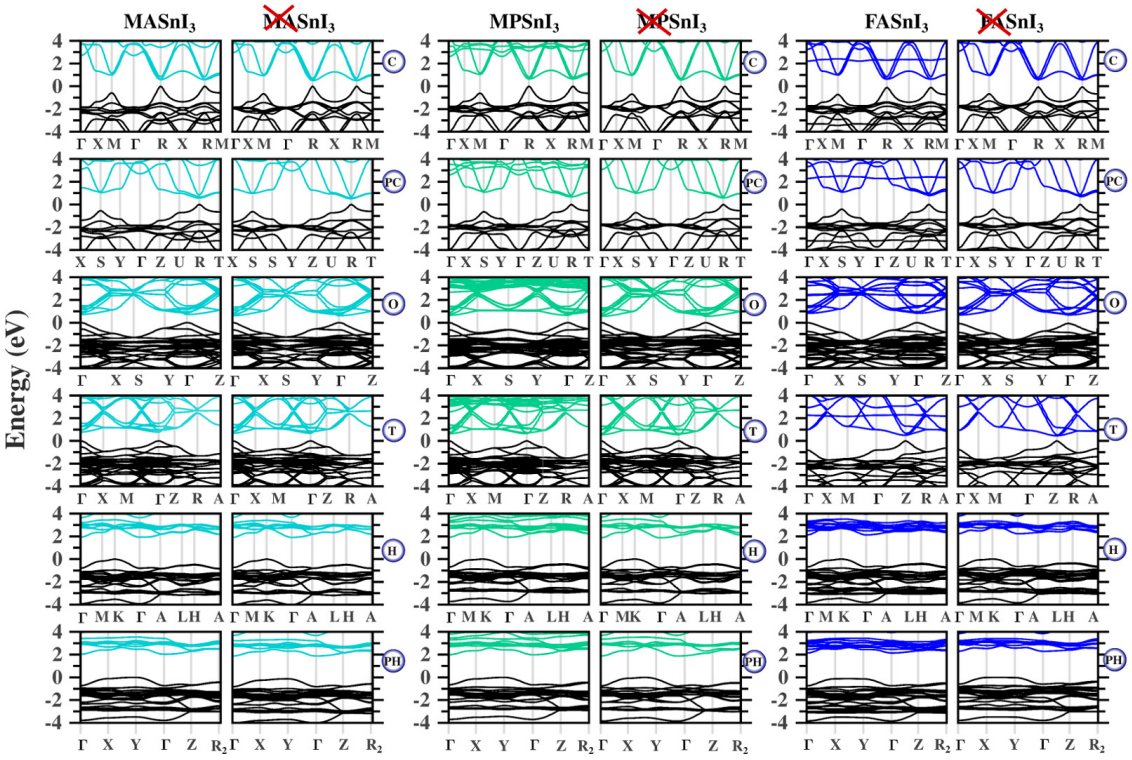

Figure S30 Band structure of cubic/pseudo-cubic (C/PC), orthorhombic (O), tetragonal (T), and hexagonal/pseudo-hexagonal (H/PH) phases of $ASnI_3$. To analyse the role of the inorganic framework, the band structure analysis of the frozen inorganic-framework were done for comparison. The top of valence band was set to zero.

Table S8 Effective mass of hole and electron for the specified lines of all the lowest ASnI$_3$ perovskites.

Cubic	**MASnI$_3$**		**MPSnI3**		**FASnI3**	
	m_h/m_0	m_e/m_0	m_h/m_0	m_e/m_0	m_h/m_0	m_e/m_0
R-Γ	-0.128	0.265	-0.134	0.239	-0.146	0.480
R-M	-0.133	0.859	-0.112	0.748	-0.156	1.074
R-X	-0.125	0.844	-0.132	0.704	-0.151	1.239
Pseudo-cubic	**MASnI$_3$**		**MPSnI$_3$**		**FASnI$_3$**	
R-U	-0.118	0.956	-0.117	0.866	-0.123	0.325
R-T	-0.132	0.603	-0.150	0.883	-0.136	1.008
Orthorhombic	**MASnI$_3$**		**MPSnI$_3$**		**FASnI$_3$**	
Γ-Z	-0.130	0.981	-0.090	0.071	-0.144	1.026
Γ-Y	-0.101	0.062	-0.125	0.900	-0.115	0.293
Γ-X	-0.126	0.672	-0.120	0.762	-0.202	1.328
Tetragonal	**MASnI$_3$**		**MPSnI$_3$**		**FASnI$_3$**	
Z-R					-0.084	0.244
Z-Γ					-0.091	0.711
Γ-M	-0.163	0.810	-0.124	0.868		
Γ-Z	-0.112	0.067	-0.080	0.055		
Γ-X	-0.137	0.640	-0.101	0.853		
Hexagonal	**MASnI$_3$**		**MPSnI$_3$**		**FASnI$_3$**	
Γ-M			-0.544	0.407		
K-Γ	-0.471	0.417	-0.695	0.422	-0.930	0.390
K-M	-0.273	0.305			-0.653	0.484
Pseudo-hexagonal	**MASnI$_3$**		**MPSnI$_3$**		**FASnI$_3$**	
Γ-X					-0.619	0.356
Γ-Y	-0.540	0.383	-0.554	-0.384	-0.584	0.433
X-Y	-5.000	0.410	-2.673	0.385		

Table S9 Average effective mass of hole and electron considering the lines indicated in Table S8 for the lowest energy ASnI$_3$ perovskites.

	MASnI$_3$		**MPSnI$_3$**		**FASnI$_3$**	
Phases	m_h/m_0	m_e/m_0	m_h/m_0	m_e/m_0	m_h/m_0	m_e/m_0
Cubic	-0.129	0.656	-0126	0.581	-0.151	0.931
Pseudo-cubic	-0.125	0.780	-0.134	0.874	-0.129	0.667
Orthorhombic	-0.120	0.572	-0.112	0.578	-0.154	0.882
Tetragonal	-0.137	0.506	-0.102	0.592	-0.088	0.478
Hexagonal	-0.372	0.361	-0.619	0.414	-0.791	0.437
Pseudo-hexagonal	-2.770	0.396	-1.613	0.384	-0.601	0.394

5 $MASnI_3$ perovskites

5.1 Cubic structures of $MASnI_3$ perovskites

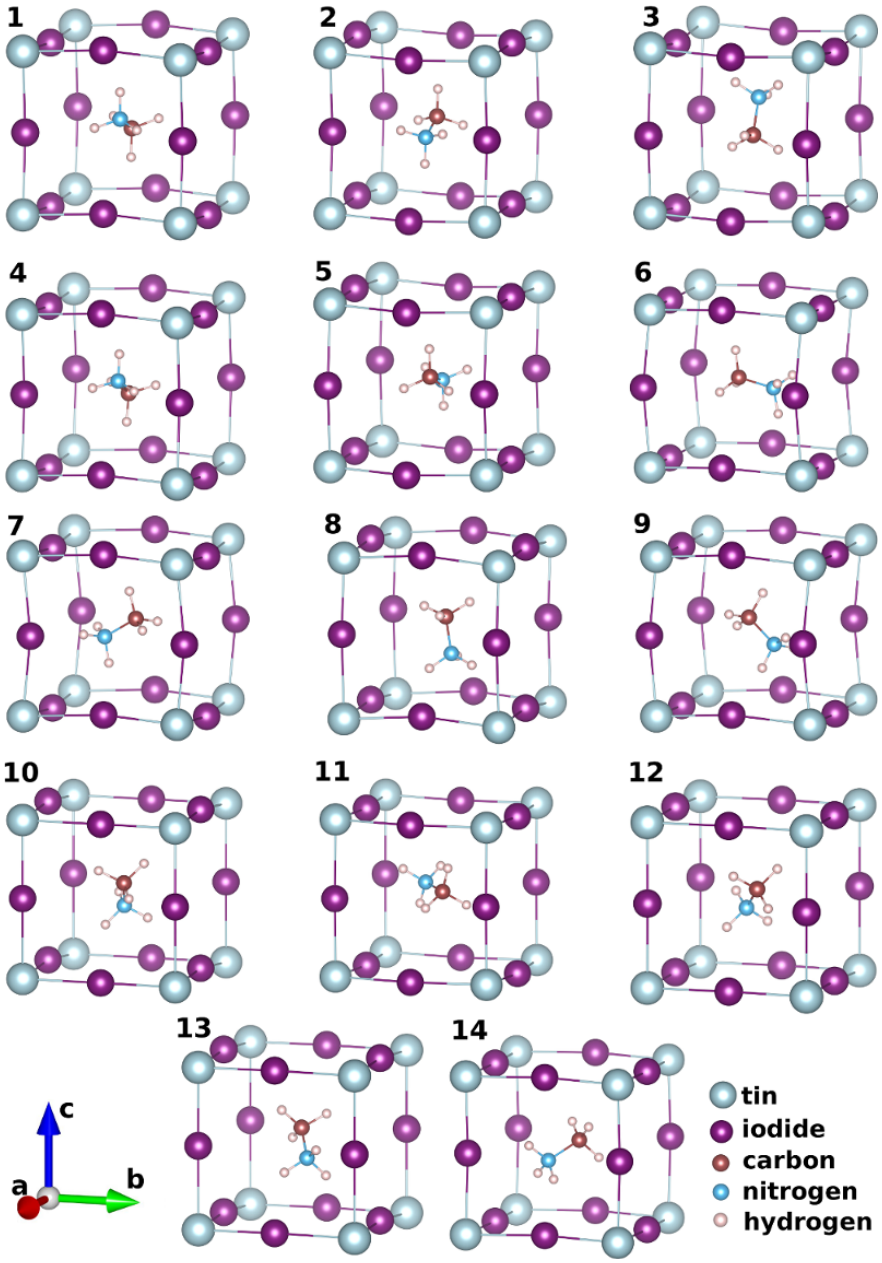

Figure S31 Orientation of organic cation in the ideal cubic structure.

Table S10 Lattice parameters of cubic phase of $MASnI_3$ perovskite, ($\alpha = \beta = \gamma = 90°$)

N	a_0 (Å)	b_0 (Å)	c_0 (Å)	N	a_0 (Å)	b_0 (Å)	c_0 (Å)
1	6.26	6.26	6.26	**8**	6.27	6.27	6.27
2	6.26	6.26	6.26	**9**	6.24	6.24	6.24
3	6.25	6.25	6.25	**10**	6.24	6.24	6.24
4	6.25	6.25	6.25	**11**	6.24	6.24	6.24
5	6.27	6.27	6.27	**12**	6.27	6.27	6.27
6	6.27	6.27	6.27	**13**	6.27	6.27	6.27
7	6.25	6.25	6.25	**14**	6.26	6.26	6.26

Table S11 Relative total energy (ΔE_{tot}), enthalpy of formation (ΔH_f^o) and cohesive energy (E_{coh}) of each $MASnI_3$ cubic structure.

N	ΔE_{tot} (meV/f.u.)	ΔH_f^o (meV/f.u.)	E_{coh} (eV/atom)	N	ΔE_{tot} (meV/f.u.)	ΔH_f^o (meV/f.u.)	E_{coh} (eV/atom)
1	0.00	−32.16	−3.28	**8**	6.72	−25.44	−3.28
2	0.21	−31.95	−3.28	**9**	20.11	−12.04	−3.28
3	0.58	−31.58	−3.28	**10**	21.50	−10.65	−3.28
4	0.75	−31.41	−3.28	**11**	22.17	−9.99	−3.28
5	2.10	−30.06	−3.28	**12**	22.99	−9.17	−3.28
6	2.80	−29.35	−3.28	**13**	23.87	−8.29	−3.28
7	3.10	−29.06	−3.28	**14**	23.94	−8.22	−3.28

5.2 Pseudo-cubic structures of $MASnI_3$ perovskites

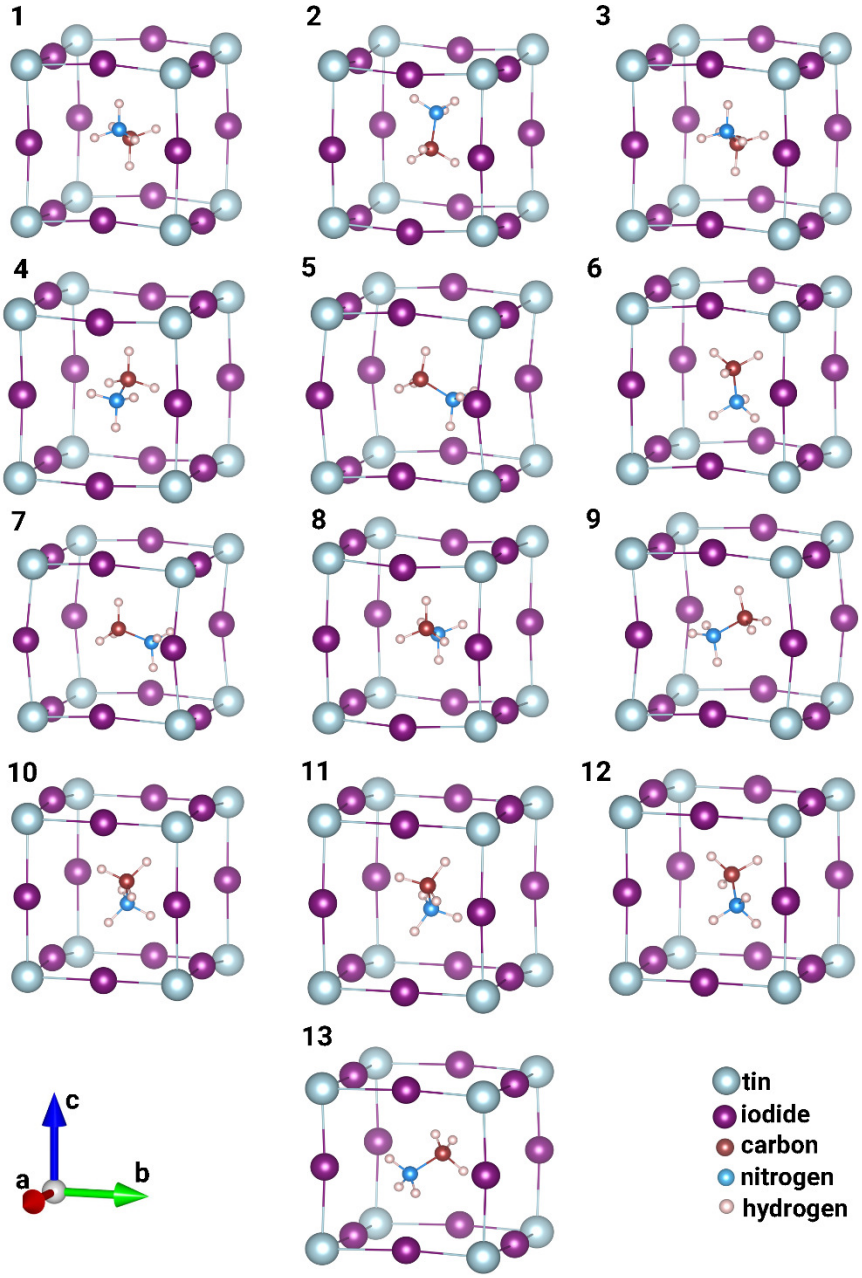

Figure S32 Orientation of organic cation in the pseudo-cubic structures.

Table S12 Lattice parameters of pseudo-cubic of $MASnI_3$ perovskite, ($\alpha = \beta = \gamma = 90°$)

N	a_0 (Å)	b_0 (Å)	c_0 (Å)	N	a_0 (Å)	b_0 (Å)	c_0 (Å)
1	6.29	6.20	6.29	**8**	6.30	6.21	6.29
2	6.29	6.20	6.29	**9**	6.19	6.27	6.29
3	6.29	6.20	6.29	**10**	6.28	6.18	6.28
4	6.29	6.20	6.29	**11**	6.26	6.18	6.28
5	6.19	6.28	6.29	**12**	6.28	6.22	6.28
6	6.29	6.21	6.30	**13**	6.27	6.29	6.25
7	6.21	6.30	6.29	**14**			

Table S13 Relative total energy (ΔE_{tot}), enthalpy of formation (ΔH_f^o) and cohesive energy (E_{coh}) of each $MASnI_3$ pseudo-cubic structure.

N	ΔE_{tot} (meV/f.u.)	ΔH_f^o (meV/f.u.)	E_{coh} (eV/atom)	N	ΔE_{tot} (meV/f.u.)	ΔH_f^o (meV/f.u.)	E_{coh} (eV/atom)
1	0.00	−35.65	−3.28	**8**	1.40	−34.25	−3.28
2	0.03	−35.62	−3.28	**9**	1.56	−34.10	−3.28
3	0.28	−35.37	−3.28	**10**	20.91	−14.74	−3.28
4	0.38	−35.27	−3.28	**11**	21.12	−14.53	−3.28
5	0.52	−35.13	−3.28	**12**	25.08	−10.57	−3.28
6	0.64	−35.01	−3.28	**13**	27.32	−8.34	−3.28
7	1.04	−34.61	−3.28				

5.3 Orthorhombic structures of $MASnI_3$ perovskites

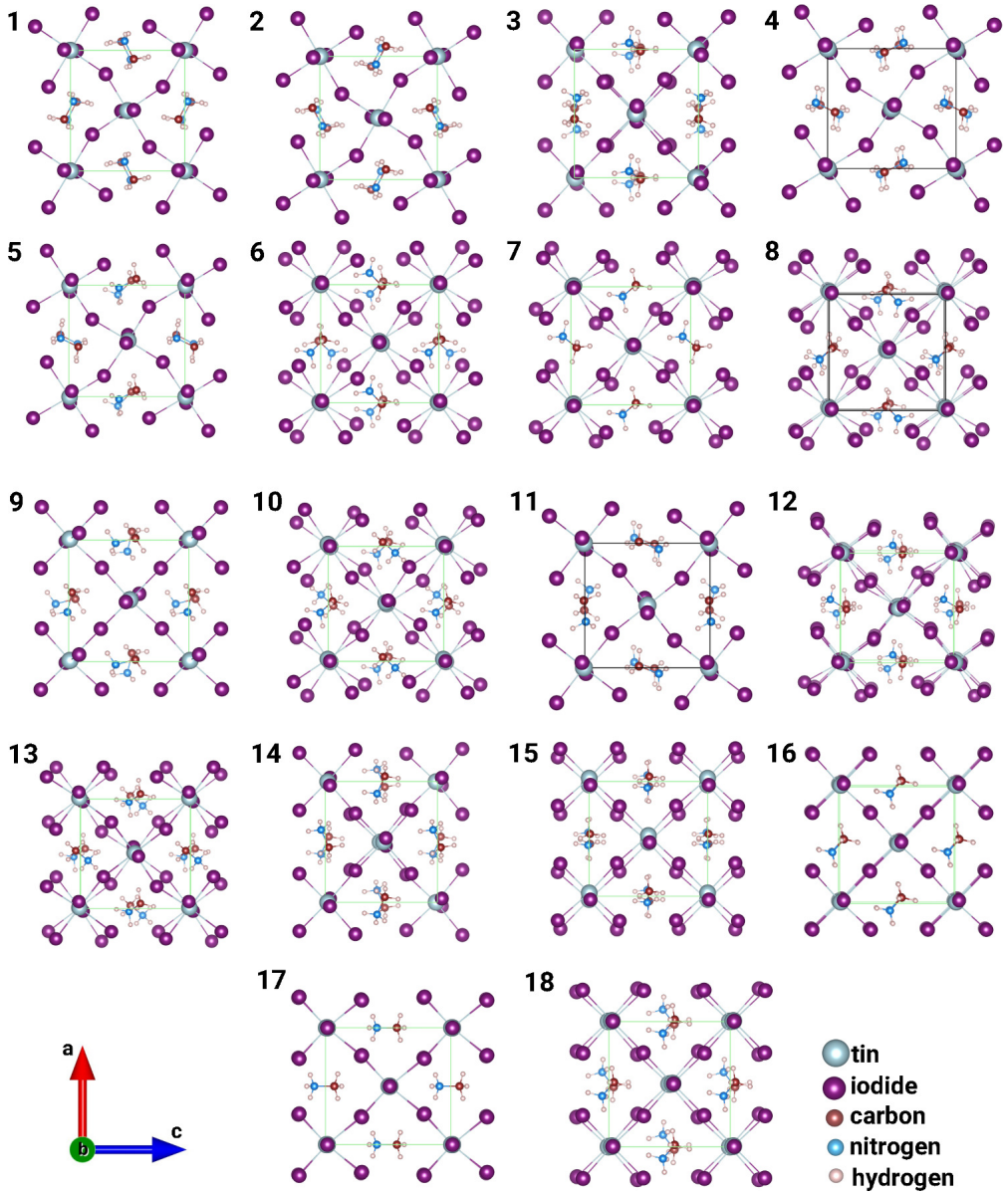

Figure S33 Orientation of organic cation in the orthorhombic structures.

Table S14 Lattice parameters of orthorhombic phase of $MASnI_3$ perovskite, ($\alpha = \beta = \gamma = 90°$)

N	a_0 (Å)	b_0 (Å)	c_0 (Å)	N	a_0 (Å)	b_0 (Å)	c_0 (Å)
1	8.91	12.54	8.45	**10**	8.72	12.57	8.75
2	8.88	12.54	8.45	**11**	8.76	12.38	8.83
3	8.95	12.41	8.67	**12**	8.59	12.55	8.87
4	8.41	12.54	8.98	**13**	8.73	12.54	8.75
5	8.86	12.52	8.50	**14**	9.18	12.38	8.52
6	8.69	12.71	8.69	**15**	8.66	12.60	8.93
7	8.65	12.59	8.79	**16**	8.86	12.60	8.75
8	8.72	12.63	8.70	**17**	8.56	12.37	9.17
9	8.91	12.26	8.79	**18**	8.94	12.54	8.67

Table S15 Relative total energy (ΔE_{tot}), enthalpy of formation (ΔH_f^o) and cohesive energy (E_{coh}) of each $MASnI_3$ orthorhombic structure.

N	ΔE_{tot} (meV/f.u.)	ΔH_f^o (meV/f.u.)	E_{coh} (eV/atom)	N	ΔE_{tot} (meV/f.u.)	ΔH_f^o (meV/f.u.)	E_{coh} (eV/atom)
1	0.00	−134.57	−3.29	**10**	37.86	−96.71	−3.28
2	0.26	−134.31	−3.29	**11**	42.12	−92.45	−3.28
3	5.72	−128.85	−3.29	**12**	50.12	−84.45	−3.28
4	15.03	−119.53	−3.28	**13**	62.35	−72.22	−3.28
5	19.35	−115.22	−3.28	**14**	79.02	−55.55	−3.28
6	26.33	−108.23	−3.28	**15**	92.28	−42.29	−3.28
7	30.45	−104.12	−3.28	**16**	96.17	−39.39	−3.28
8	35.56	−99.00	−3.28	**17**	103.96	−30.60	−3.28
9	36.09	−98.48	−3.28	**18**	107.77	−26.79	−3.28

5.4 Tetragonal structures of $MASnI_3$ perovskites

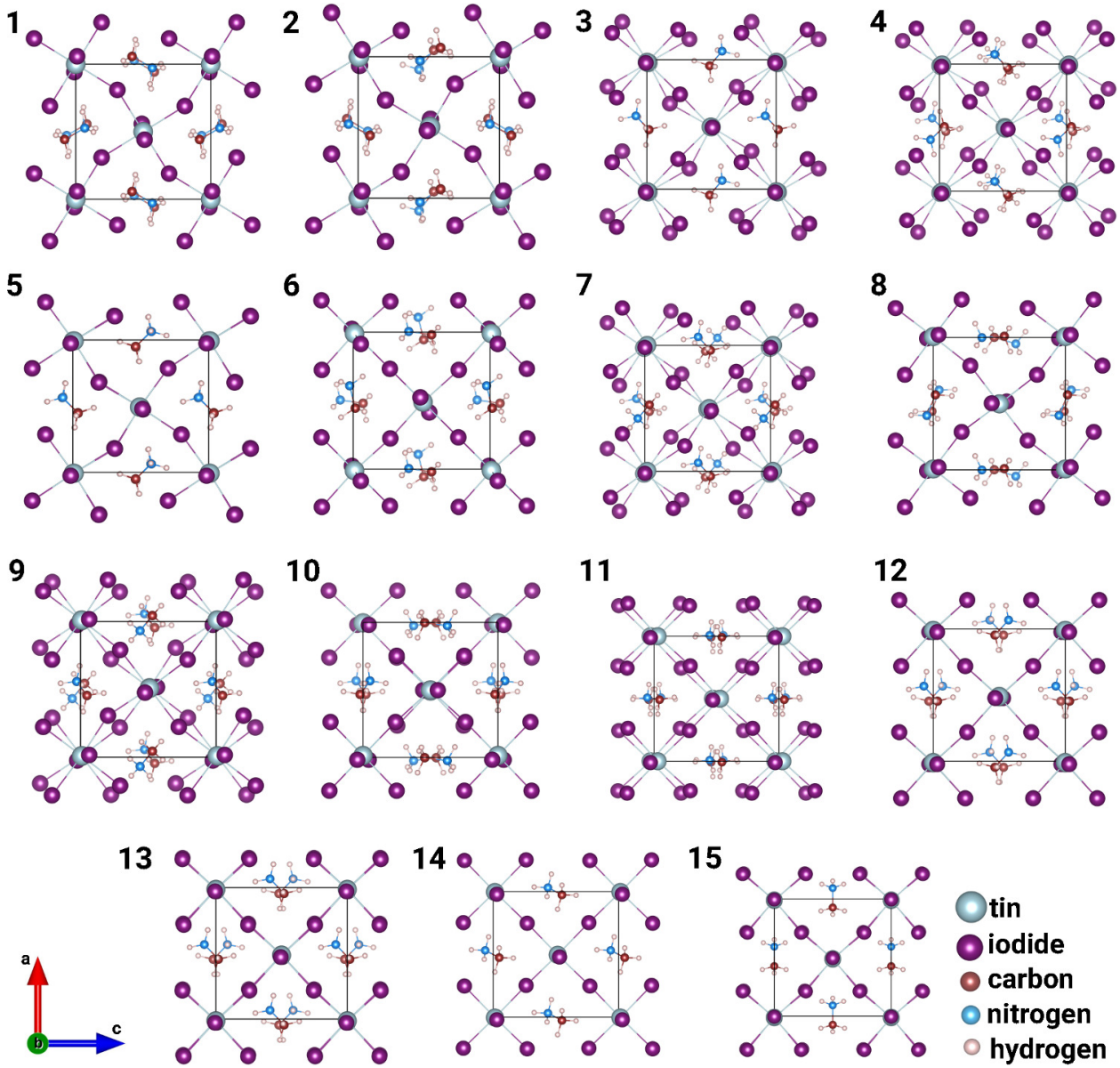

Figure S34 Orientation of organic cation in tetragonal structures.

Table S16 Lattice parameters of tetragonal phase of $MASnI_3$ perovskite, ($\alpha = \beta = \gamma = 90°$)

N	a_0 (Å)	b_0 (Å)	c_0 (Å)	N	a_0 (Å)	b_0 (Å)	c_0 (Å)
1	8.67	8.67	12.50	**9**	8.74	8.74	12.53
2	8.67	8.67	12.52	**10**	8.81	8.81	12.42
3	8.72	8.72	12.60	**11**	8.79	8.79	12.61
4	8.71	8.71	12.63	**12**	8.82	8.82	12.53
5	8.68	8.68	12.63	**13**	8.81	8.81	12.57
6	8.85	8.85	12.26	**14**	8.80	8.80	12.58
7	8.73	8.73	12.57	**15**	8.86	8.86	12.35
8	8.78	8.78	12.40				

Table S17 Relative total energy (ΔE_{tot}), enthalpy of formation (ΔH_f^o) and cohesive energy (E_{coh}) of each $MASnI_3$ pseudo-cubic structure.

N	ΔE_{tot} (meV/f.u.)	ΔH_f^o (meV/f.u.)	E_{coh} (eV/atom)	N	ΔE_{tot} (meV/f.u.)	ΔH_f^o (meV/f.u.)	E_{coh} (eV/atom)
1	0.00	−121.67	−3.28	**9**	49.31	−72.36	−3.28
2	8.91	−112.76	−3.28	**10**	59.01	−62.66	−3.28
3	18.66	−103.02	−3.28	**11**	83.23	−38.44	−3.28
4	22.20	−99.47	−3.28	**12**	86.29	−35.38	−3.28
5	24.62	−97.06	−3.28	**13**	88.78	−32.89	−3.28
6	24.86	−96.82	−3.28	**14**	102.56	−19.12	−3.28
7	25.16	−96.51	−3.28	**15**	108.16	−13.51	−3.28
8	28.93	−92.75	−3.28				

5.5 Pseudo-hexagonal structures of $MASnI_3$ perovskites

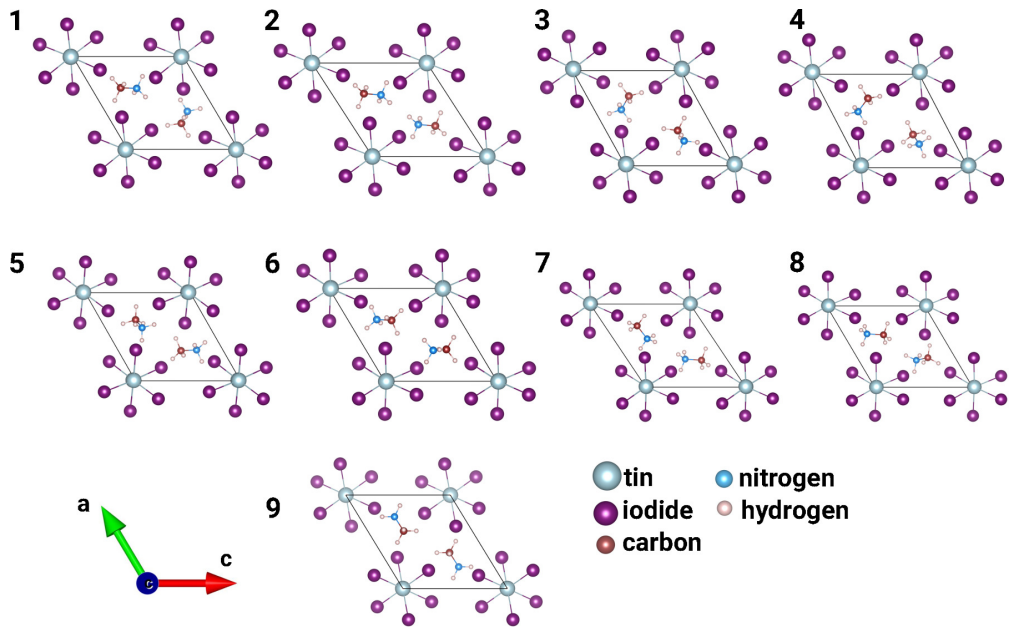

Figure S35 Orientation of organic cation in the pseudo-hexagonal structures.

Table S18 Lattice parameters of pseudo-hexagonal phase of $MASnI_3$ perovskite

N	a_0 Å	b_0 Å	c_0 Å	α deg	β deg	γ deg	N	a_0 Å	b_0 Å	c_0 Å	α deg	β deg	γ deg
1	8.72	8.46	7.71	92.55	96.68	119.97	**6**	8.79	8.42	7.79	96.07	80.87	121.38
2	8.92	8.54	7.69	91.30	98.40	122.28	**7**	8.74	8.74	7.79	95.80	95.82	122.75
3	8.45	8.59	7.75	98.83	89.04	118.77	**8**	8.80	8.44	7.78	82.98	99.46	121.20
4	8.51	8.50	7.75	100.74	86.44	117.65	**9**	8.47	8.88	7.67	90.00	90.00	121.39
5	8.74	8.49	7.77	100.26	81.23	120.57							

Table S19 Relative total energy (ΔE_{tot}), enthalpy of formation (ΔH_f^o) and cohesive energy (E_{coh}) of each pseudo-hexagonal $MASnI_3$ structure.

N	ΔE_{tot} (meV/f.u.)	ΔH_f^o (meV/f.u.)	E_{coh} (eV/atom)	N	ΔE_{tot} (meV/f.u.)	ΔH_f^o (meV/f.u.)	E_{coh} (eV/atom)
1	0.00	−94.14	−3.28	**6**	12.80	−81.35	−3.28
2	0.60	−93.54	−3.28	**7**	37.43	−56.71	−3.28
3	2.17	−91.97	−3.28	**8**	42.82	−51.33	−3.28
4	3.11	−91.04	−3.28	**9**	43.27	−50.87	−3.28
5	7.86	−86.28	−3.28				

5.6 Hexagonal structures of $MASnI_3$ perovskites

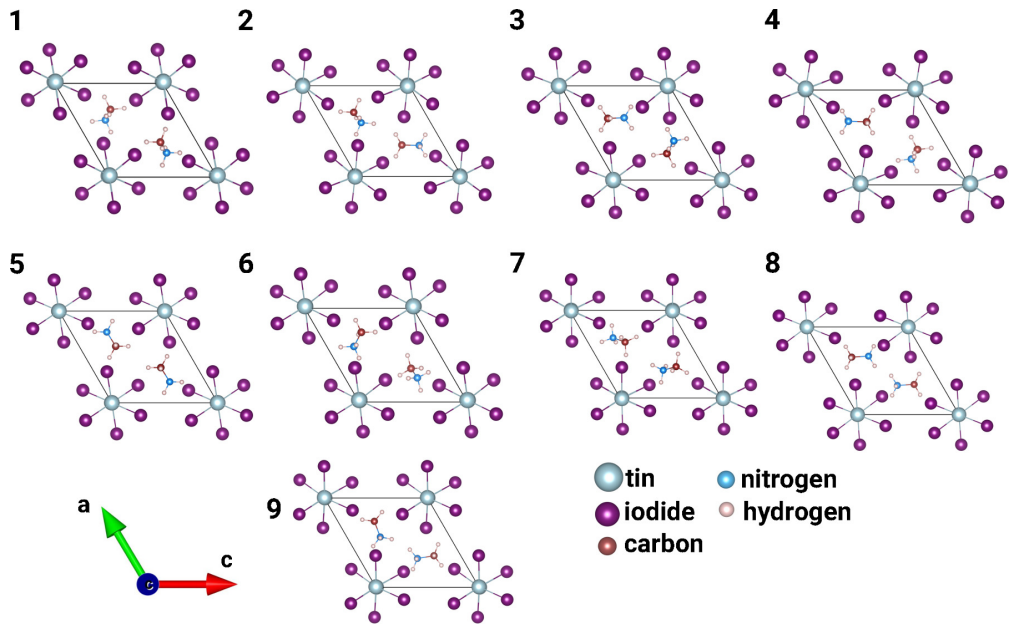

Figure S36 Orientation of organic cation in the hexagonal structures.

Table S20 Lattice parameters of hexagonal phase of $MASnI_3$ perovskite

N	a_0 (Å)	b_0 (Å)	c_0 (Å)	α deg	β deg	γ deg	N	a_0 Å	b_0 Å	c_0 Å	α deg	β deg	γ deg
1	8.52	8.52	7.73	90.00	90.00	120.00	**6**	8.51	8.51	7.79	90.00	90.00	120.00
2	8.62	8.62	7.58	90.00	90.00	120.00	**7**	8.61	8.61	7.58	90.00	90.00	120.00
3	8.59	8.59	7.61	90.00	90.00	120.00	**8**	8.73	8.73	7.37	90.00	90.00	120.00
4	8.62	8.62	7.57	90.00	90.00	120.00	**9**	8.74	8.74	7.39	90.00	90.00	120.00
5	8.68	8.68	7.55	90.00	90.00	120.00							

Table S21 Relative total energy (ΔE_{tot}), enthalpy of formation (ΔH_f^o) and cohesive energy (E_{coh}) of each $MASnI_3$ cubic structure.

N	ΔE_{tot} (meV/f.u.)	ΔH_f^o (meV/f.u.)	E_{coh} (eV/atom)	N	ΔE_{tot} (meV/f.u.)	ΔH_f^o (meV/f.u.)	E_{coh} (eV/atom)
1	0.00	−38.64	−3.28	**6**	13.98	−24.66	−3.28
2	2.20	−36.44	−3.28	**7**	17.53	−21.11	−3.28
3	5.15	−33.49	−3.28	**10**	29.38	−9.26	−3.28
4	10.58	−28.06	−3.28	**11**	52.56	13.92	−3.28
5	10.99	−27.65	−3.28				

6 $MPSnI_3$ perovskites

6.1 Cubic structures of $MPSnI_3$ perovskites

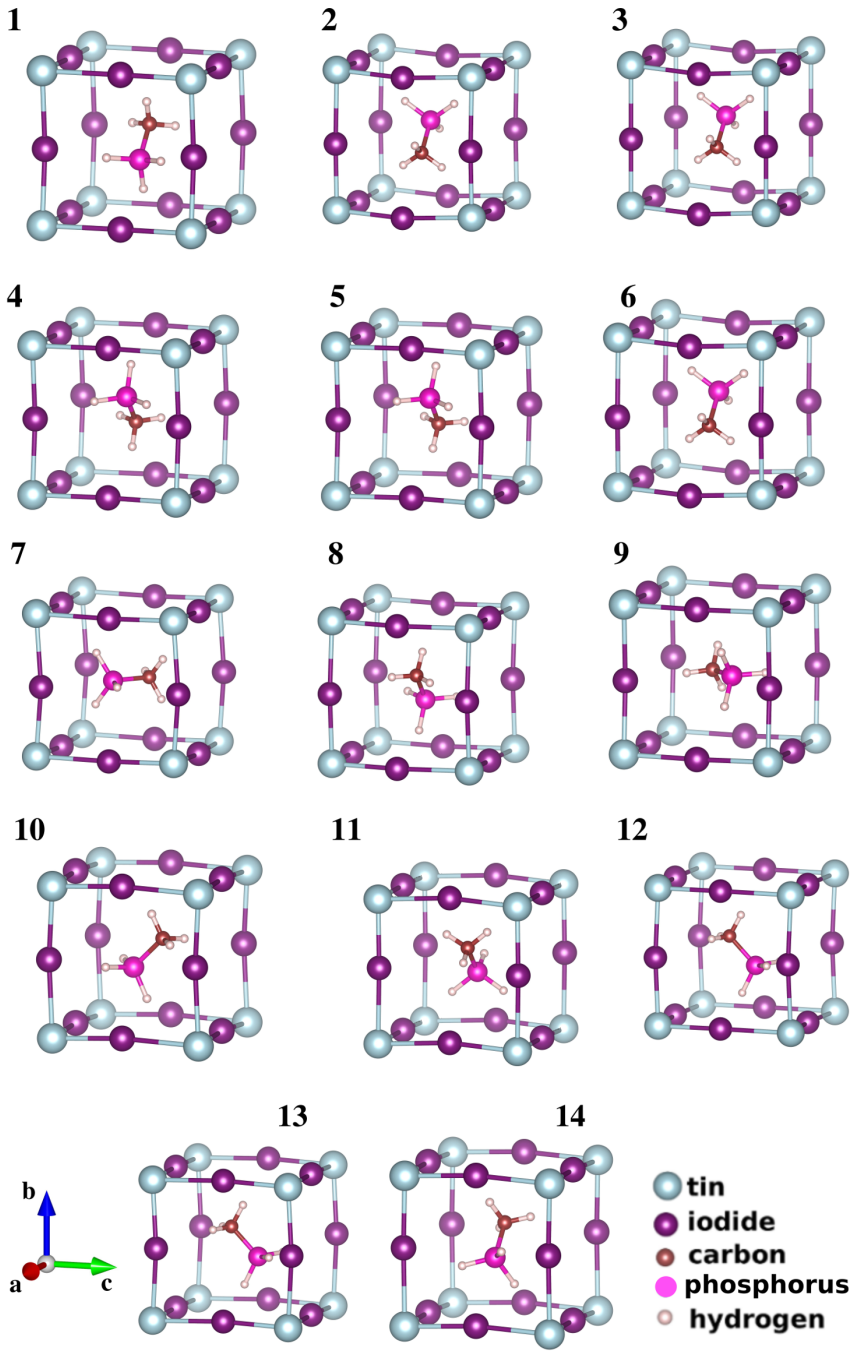

Figure S37 Orientation of organic cation in the cubic structures.

Table S22 Relative total energy (ΔE_{tot}), enthalpy of formation (ΔH_f^o) and cohesive energy (E_{coh}) of each $MPSnI_3$ cubic structure.

N	ΔE_{tot} (meV/f.u.)	ΔH_f^o (meV/f.u.)	E_{coh} (eV/atom)	N	ΔE_{tot} (meV/f.u.)	ΔH_f^o (meV/f.u.)	E_{coh} (eV/atom)
1	0.00	−77.86	−2.93	**8**	0.88	−76.98	−2.93
2	0.01	−77.85	−2.93	**9**	0.94	−76.92	−2.93
3	0.29	−77.57	−2.93	**10**	1.10	−76.76	−2.93
4	0.45	−77.41	−2.93	**11**	1.18	−76.67	−2.93
5	0.52	−77.34	−2.93	**12**	1.31	−76.55	−2.93
6	0.70	−77.16	−2.93	**13**	1.48	−76.37	−2.93
7	0.70	−77.16	−2.93	**14**	16.69	−61.17	−2.93

Table S23 Lattice parameters of cubic phase of $MPSnI_3$ perovskite, ($\alpha = \beta = \gamma = 90°$)

N	a_0 (Å)	b_0 (Å)	c_0 (Å)	N	a_0 (Å)	b_0 (Å)	c_0 (Å)
1	6.34	6.34	6.34	**8**	6.34	6.34	6.34
2	6.34	6.34	6.34	**9**	6.33	6.33	6.33
3	6.33	6.33	6.33	**10**	6.34	6.34	6.34
4	6.34	6.34	6.34	**11**	6.33	6.33	6.33
5	6.34	6.34	6.34	**12**	6.33	6.33	6.33
6	6.34	6.34	6.34	**13**	6.34	6.34	6.34
7	6.33	6.33	6.33	**14**	6.34	6.34	6.34

6.2 Pseudo-cubic structures of $MPSnI_3$ perovskites

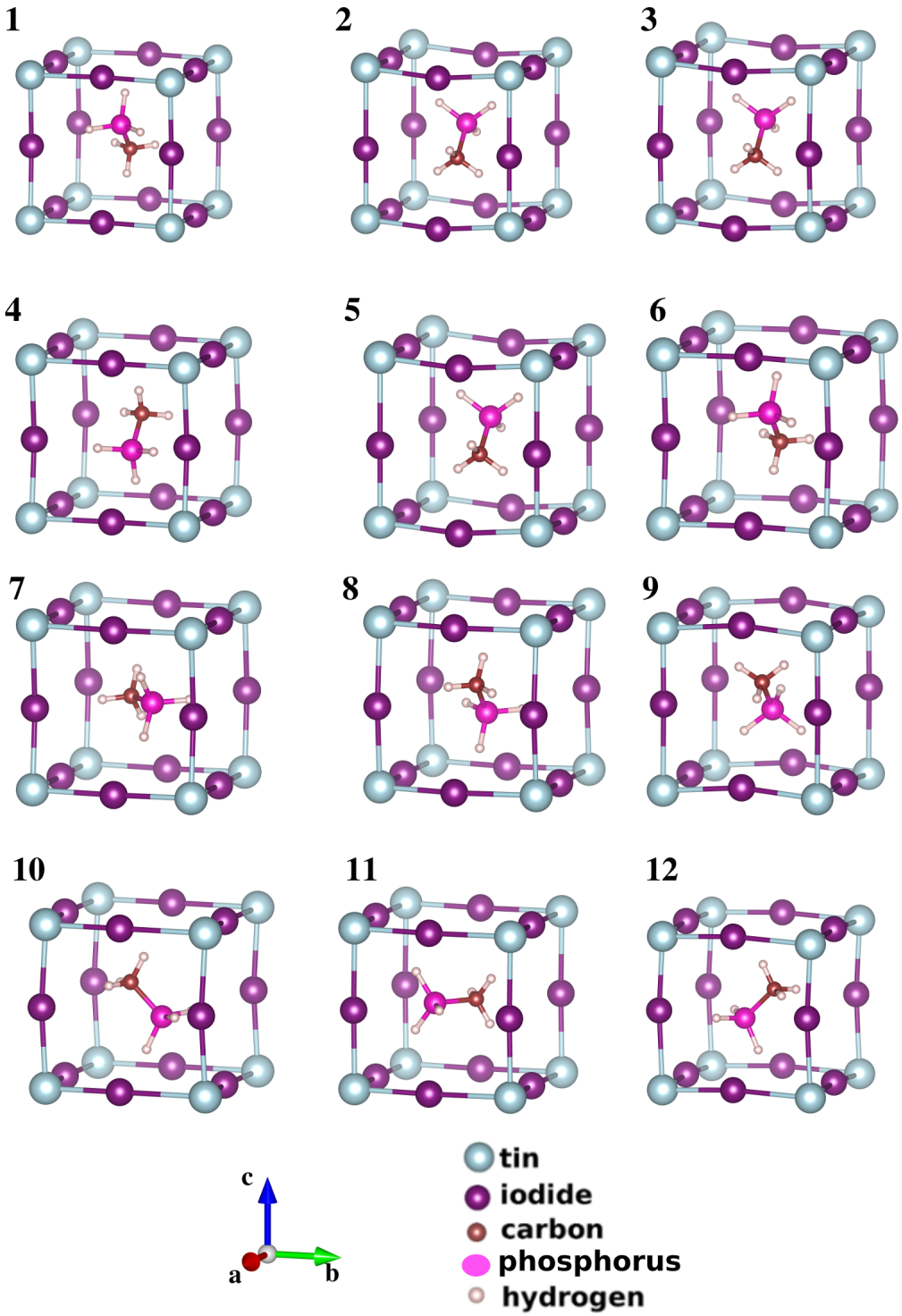

Figure S38 Orientation of organic cation in the pseudo-cubic structures.

Table S24 Relative total energy (ΔE_{tot}), enthalpy of formation (ΔH_f^o) and cohesive energy (E_{coh}) of each $MPSnI_3$ pseudo-cubic structure.

N	ΔE_{tot} (meV/f.u.)	ΔH_f^o (meV/f.u.)	E_{coh} (eV/atom)	N	ΔE_{tot} (meV/f.u.)	ΔH_f^o (meV/f.u.)	E_{coh} (eV/atom)
1	0.00	−79.43	−2.93	**7**	0.80	−78.63	−2.93
2	0.07	−79.36	−2.93	**8**	0.82	−78.61	−2.93
3	0.17	−79.26	−2.93	**9**	0.92	−78.51	−2.93
4	0.20	−79.23	−2.93	**10**	1.01	−78.42	−2.93
5	0.38	−79.05	−2.93	**11**	2.32	−77.10	−2.93
6	0.63	−78.80	−2.93	**12**	2.55	−76.88	−2.93

Table S25 Lattice parameters of pseudo-cubic phase of $MPSnI_3$ perovskite, ($\alpha = \beta = \gamma = 90°$)

N	a_0 (Å)	b_0 (Å)	c_0 (Å)	N	a_0 (Å)	b_0 (Å)	c_0 (Å)
1	6.41	6.31	6.30	**7**	6.40	6.31	6.31
2	6.31	6.30	6.40	**8**	6.39	6.31	6.31
3	6.31	6.32	6.40	**9**	6.31	6.31	6.39
4	6.39	6.32	6.31	**10**	6.31	6.40	6.31
5	6.32	6.30	6.39	**11**	6.32	6.37	6.33
6	6.39	6.31	6.31	**12**	6.33	6.34	6.33

6.3 Orthorhombic structures of $MPSnI_3$ perovskites

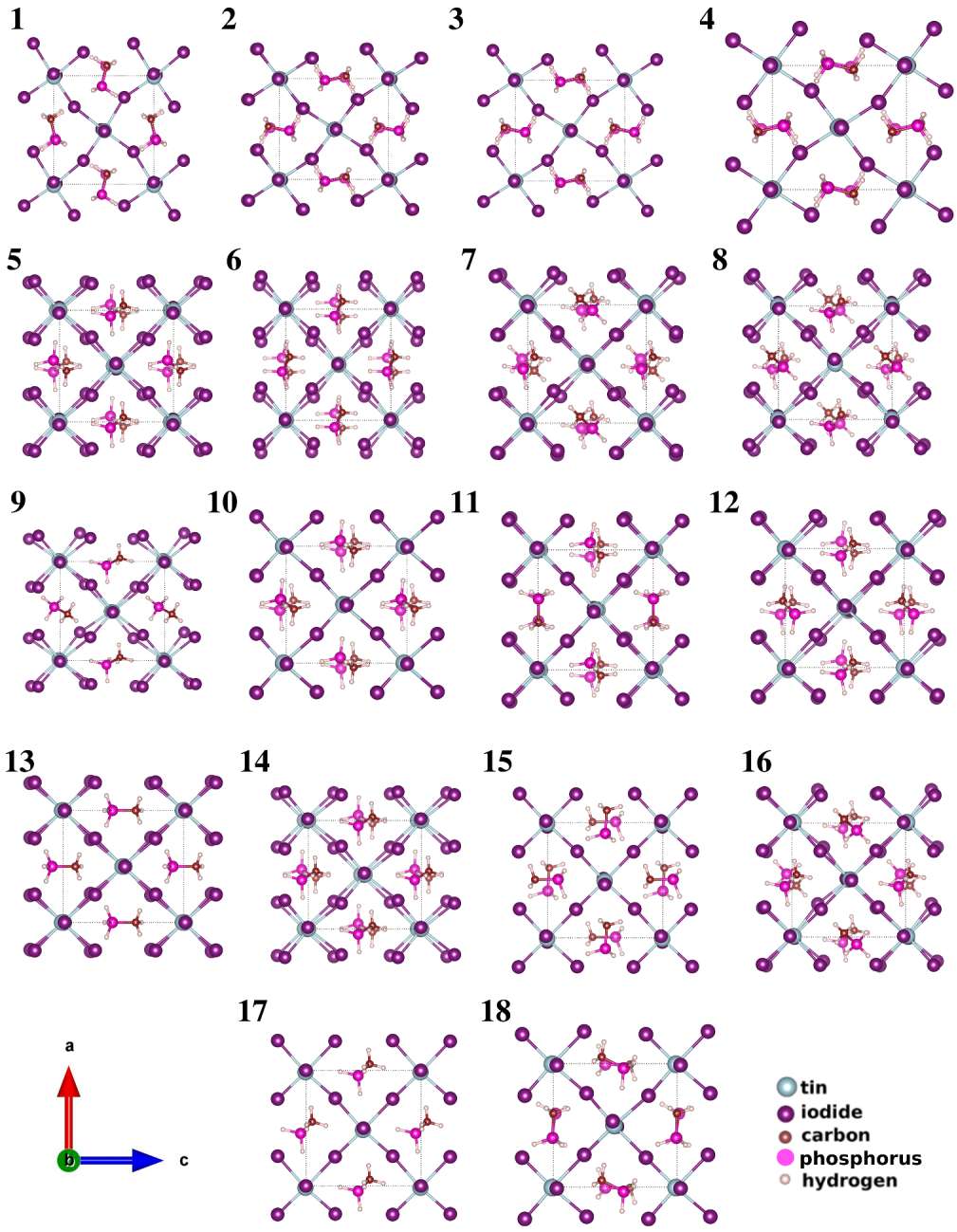

Figure S39 Orientation of organic cation in the orthorhombic structures.

Table S26 Lattice parameters of orthorhombic phase of $MPSnI_3$ perovskite, ($\alpha = \beta = \gamma = 90°$)

N	a_0 (Å)	b_0 (Å)	c_0 (Å)	N	a_0 (Å)	b_0 (Å)	c_0 (Å)
1	9.15	12.63	8.45	**10**	8.83	12.60	9.10
2	8.44	12.64	9.14	**11**	9.12	12.60	8.73
3	8.43	12.63	9.12	**12**	8.97	12.56	8.97
4	8.44	12.62	9.12	**13**	8.60	12.69	9.27
5	8.85	12.52	9.02	**14**	8.78	12.53	9.15
6	9.22	12.55	8.71	**15**	8.93	12.63	8.91
7	8.90	12.66	8.92	**16**	8.95	12.64	8.92
8	8.91	12.71	8.94	**17**	8.99	12.62	8.95
9	8.72	12.56	8.17	**18**	8.94	12.59	8.97

Table S27 Relative total energy (ΔE_{tot}), enthalpy of formation (ΔH_f^o) and cohesive energy (E_{coh}) of each $MPSnI_3$ orthorhombic structure.

N	ΔE_{tot} (meV/f.u.)	ΔH_f^o (meV/f.u.)	E_{coh} (eV/atom)	N	ΔE_{tot} (meV/f.u.)	ΔH_f^o (meV/f.u.)	E_{coh} (eV/atom)
1	0.00	−174.48	−2.94	**10**	73.06	−101.42	−2.93
2	6.14	−168.34	−2.94	**11**	75.01	−99.47	−2.93
3	6.56	−167.92	−2.94	**12**	75.71	−98.77	−2.93
4	6.72	−167.76	−2.93	**13**	79.95	−94.53	−2.93
5	61.11	−113.37	−2.93	**14**	82.04	−92.45	−2.93
6	63.17	−111.32	−2.93	**15**	83.01	−91.47	−2.93
7	63.89	−110.59	−2.93	**16**	88.84	−85.64	−2.93
8	70.85	−103.63	−2.93	**17**	93.76	−80.72	−2.93
9	71.74	−102.74	−2.93	**18**	97.11	−77.38	−2.93

6.4 Tetragonal structures of $MPSnI_3$ perovskites

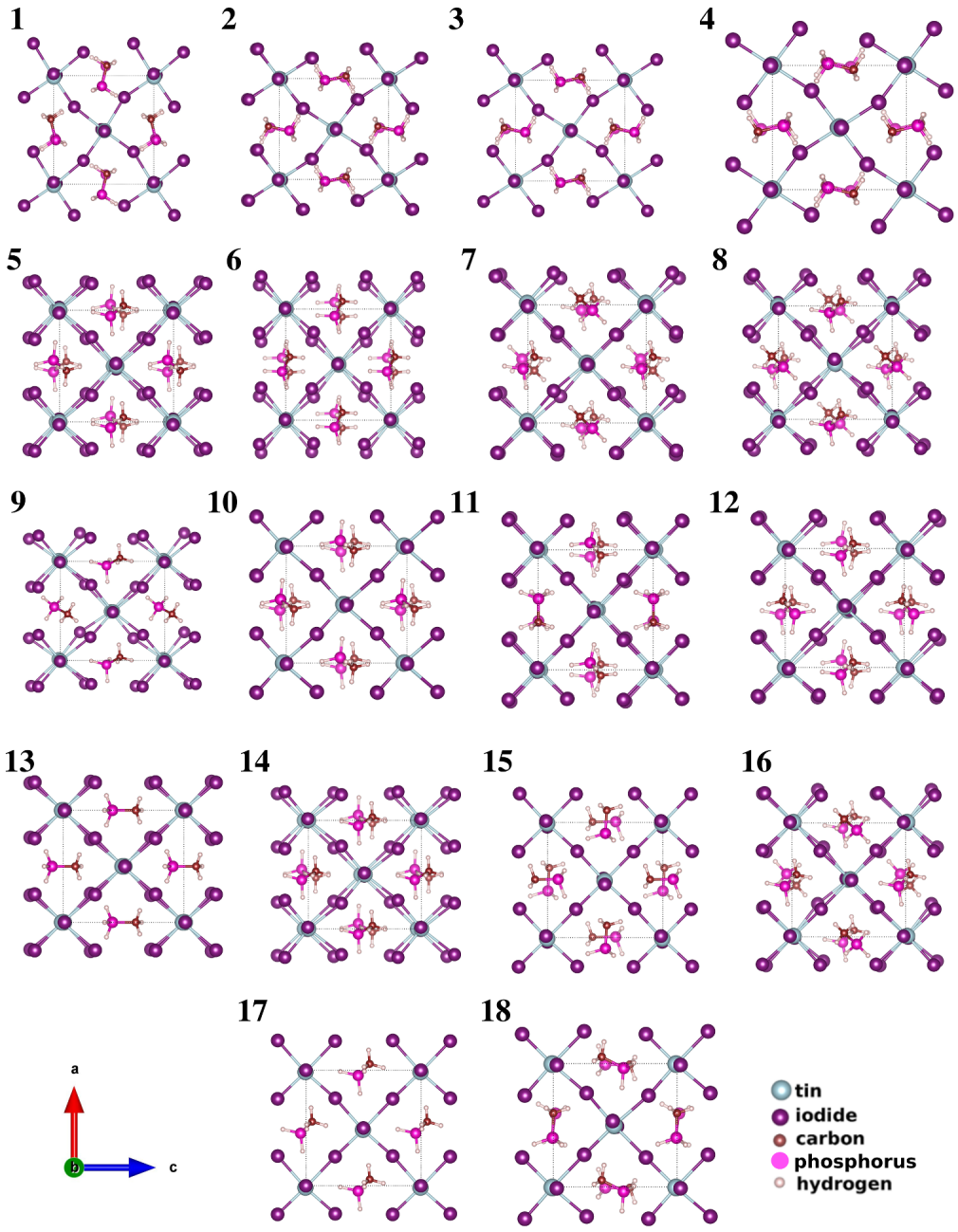

Figure S40 Orientation of organic cation in the tetragonal structures.

Table S28 Lattice parameters of tetragonal phase of $MPSnI_3$ perovskite, ($\alpha = \beta = \gamma = 90°$)

N	a_0 (Å)	b_0 (Å)	c_0 (Å)	N	a_0 (Å)	b_0 (Å)	c_0 (Å)
1	8.83	8.83	12.57	**9**	8.94	8.94	12.61
2	8.91	8.91	12.66	**10**	8.94	8.94	12.61
3	8.93	8.93	12.53	**11**	8.94	8.94	12.68
4	8.94	8.94	12.59	**12**	8.96	8.96	12.56
5	8.93	8.93	12.71	**13**	8.96	8.96	12.63
6	8.96	8.96	12.59	**14**	8.95	8.95	12.59
7	8.93	8.93	12.58	**15**	8.96	8.96	12.63
8	8.95	8.95	12.61				

Table S29 Relative total energy (ΔE_{tot}), enthalpy of formation (ΔH_f^o) and cohesive energy (E_{coh}) of each $MPSnI_3$ tetragonal structure.

N	ΔE_{tot} (meV/f.u.)	ΔH_f^o (meV/f.u.)	E_{coh} (eV/atom)	N	ΔE_{tot} (meV/f.u.)	ΔH_f^o (meV/f.u.)	E_{coh} (eV/atom)
1	0.00	−130.91	2.93	**9**	42.21	−88.69	2.93
2	20.36	−110.54	2.93	**10**	42.34	−88.57	2.93
3	20.90	−110.01	2.93	**11**	42.92	−87.98	2.93
4	27.32	−103.59	2.93	**12**	46.81	−84.10	2.93
5	27.46	−103.44	2.93	**13**	49.94	−80.96	2.93
6	33.98	−96.93	2.93	**14**	53.54	−77.37	2.93
7	36.57	−94.34	2.93	**15**	66.01	−64.90	2.93
8	37.76	−93.14	2.93				

6.5 Pseudo-hexagonal structures of $MPSnI_3$ perovskites

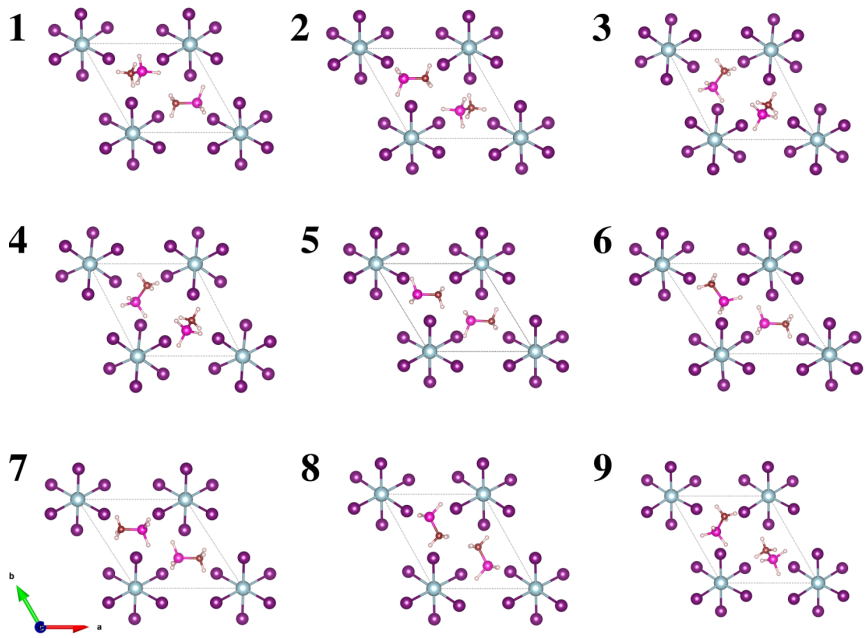

Figure S41 Orientation of organic cation in the pseudo-hexagonal structures.

Table S30 Lattice parameters of pseudo-hexagonal phase of $MPSnI_3$ perovskite

N	a_0 Å	b_0 Å	c_0 Å	α deg	β deg	γ deg	N	a_0 Å	b_0 Å	c_0 Å	α deg	β deg	γ deg
1	9.06	8.59	7.69	94.32	86.92	119.84	**6**	9.07	9.07	7.60	87.29	87.28	123.17
2	9.06	8.60	7.70	85.51	93.14	119.99	**7**	9.14	9.00	7.58	85.41	89.80	122.90
3	8.79	8.67	7.66	94.32	91.82	117.12	**8**	8.64	9.14	7.48	90.00	90.00	119.04
4	8.78	8.68	7.66	94.35	91.95	117.13	**9**	8.69	8.99	7.73	96.90	90.96	119.40
5	9.11	8.88	7.41	90.42	89.65	121.48							

Table S31 Relative total energy (ΔE_{tot}), enthalpy of formation (ΔH_f^o) and cohesive energy (E_{coh}) of each $MPSnI_3$ pseudo-hexagonal structure.

N	ΔE_{tot} (meV/f.u.)	ΔH_f^o (meV/f.u.)	E_{coh} (eV/atom)	N	ΔE_{tot} (meV/f.u.)	ΔH_f^o (meV/f.u.)	E_{coh} (eV/atom)
1	0.00	−89.43	−2.93	**6**	19.33	−70.10	−2.93
2	0.12	−89.32	−2.93	**7**	24.02	−65.42	−2.93
3	6.77	−82.66	−2.93	**8**	30.92	−58.51	−2.93
4	7.12	−82.32	−2.93	**9**	31.92	−57.52	−2.93
5	16.18	−73.25	−2.93				

6.6 Hexagonal structures of $MPSnI_3$ perovskites

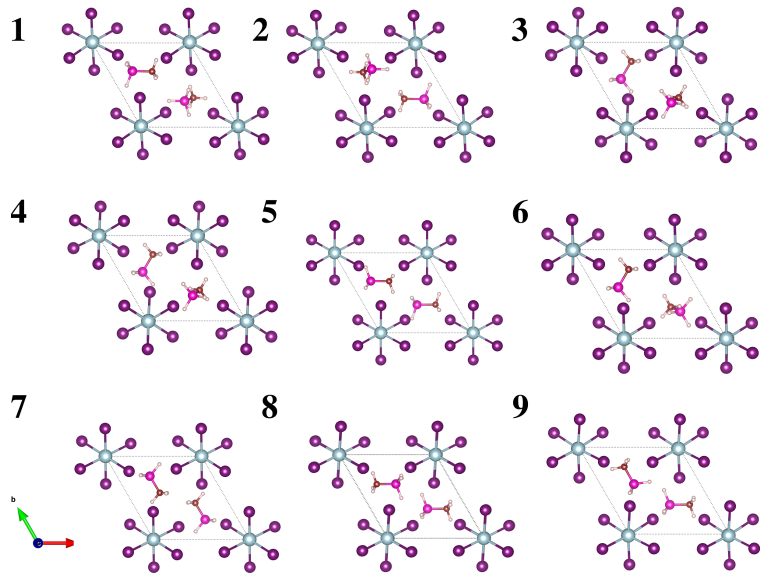

Figure S42 Orientation of organic cation in the hexagonal structures.

Table S32 Lattice parameters of hexagonal phase of $MPSnI_3$ perovskite

N	a_0 Å	b_0 Å	c_0 Å	α deg	β deg	γ deg	N	a_0 Å	b_0 Å	c_0 Å	α deg	β deg	γ deg
1	8.83	8.83	7.67	90.00	90.00	120.00	**6**	8.84	8.84	7.69	90.00	90.00	120.00
2	8.82	8.82	7.67	90.00	90.00	120.00	**7**	8.89	8.89	7.55	90.00	90.00	120.00
3	8.73	8.73	7.83	90.00	90.00	120.00	**8**	9.07	9.07	7.31	90.00	90.00	120.00
4	8.73	8.73	7.82	90.00	90.00	120.00	**9**	9.07	9.07	7.31	90.00	90.00	120.00
5	9.00	9.00	7.30	90.00	90.00	120.00							

Table S33 Relative total energy (ΔE_{tot}), enthalpy of formation (ΔH_f^o) and cohesive energy (E_{coh}) of each $MPSnI_3$ hexagonal structure.

N	ΔE_{tot} (meV/f.u.)	ΔH_f^o (meV/f.u.)	E_{coh} (eV/atom)	N	ΔE_{tot} (meV/f.u.)	ΔH_f^o (meV/f.u.)	E_{coh} (eV/atom)
1	0.00	−67.73	−2.93	**6**	10.81	−56.92	−2.93
2	0.08	−67.65	−2.93	**7**	29.48	−38.25	−2.92
3	6.41	−61.32	−2.93	**8**	38.74	−28.99	−2.92
4	7.11	−60.62	−2.93	**9**	39.11	−28.62	−2.92
5	8.73	−59.00	−2.93				

7 $FASnI_3$ perovskites

7.1 Cubic structures of $FASnI_3$ perovskites

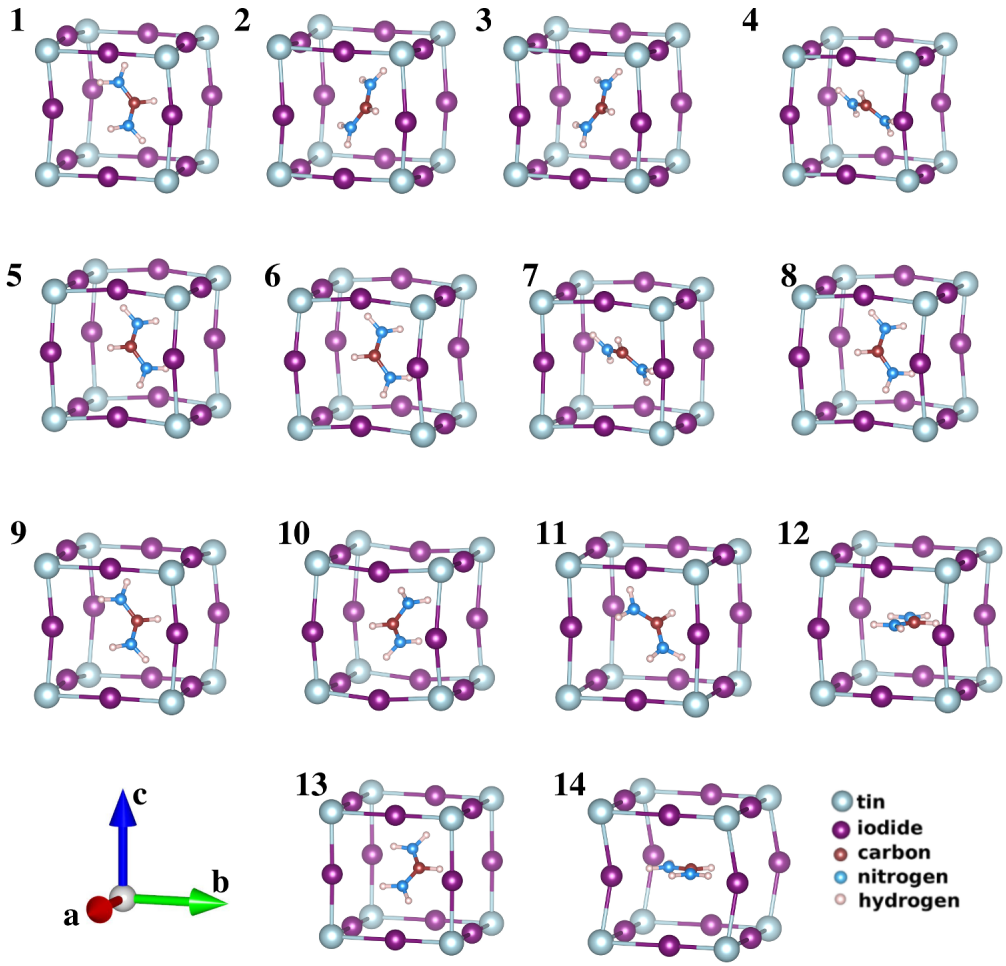

Figure S43 Orientation of organic cation in the cubic structures.

Table S34 Lattice parameters of cubic phase of $FASnI_3$ perovskite, ($\alpha = \beta = \gamma = 90°$)

N	a_0 (Å)	b_0 (Å)	c_0 (Å)	N	a_0 (Å)	b_0 (Å)	c_0 (Å)
1	6.35	6.35	6.35	**8**	6.34	6.34	6.34
2	6.35	6.35	6.35	**9**	6.35	6.35	6.35
3	6.35	6.35	6.35	**10**	6.34	6.34	6.34
4	6.34	6.34	6.34	**11**	6.41	6.41	6.41
5	6.35	6.35	6.35	**12**	6.32	6.32	6.32
6	6.34	6.34	6.34	**13**	6.39	6.39	6.39
7	6.35	6.35	6.35	**14**	6.42	6.42	6.42

Table S35 Relative total energy (ΔE_{tot}), enthalpy of formation (ΔH_f^o) and cohesive energy (E_{coh}) of each $FASnI_3$ cubic structure.

N	ΔE_{tot} (meV/f.u.)	ΔH_f^o (meV/f.u.)	E_{coh} (eV/atom)	N	ΔE_{tot} (meV/f.u.)	ΔH_f^o (meV/f.u.)	E_{coh} (eV/atom)
1	0.00	40.17	−3.68	**8**	0.69	40.86	−3.68
2	0.09	40.26	−3.68	**9**	0.70	40.87	−3.68
3	0.43	40.60	−3.68	**10**	0.80	40.98	−3.68
4	0.44	40.61	−3.68	**11**	38.86	79.03	−3.67
5	0.44	40.61	−3.68	**12**	108.38	148.55	−3.67
6	0.56	40.73	−3.68	**13**	131.27	171.44	−3.67
7	0.58	40.75	−3.68	**14**	135.64	175.81	−3.66

7.2 Pseudo-cubic structures of $FASnI_3$ perovskites

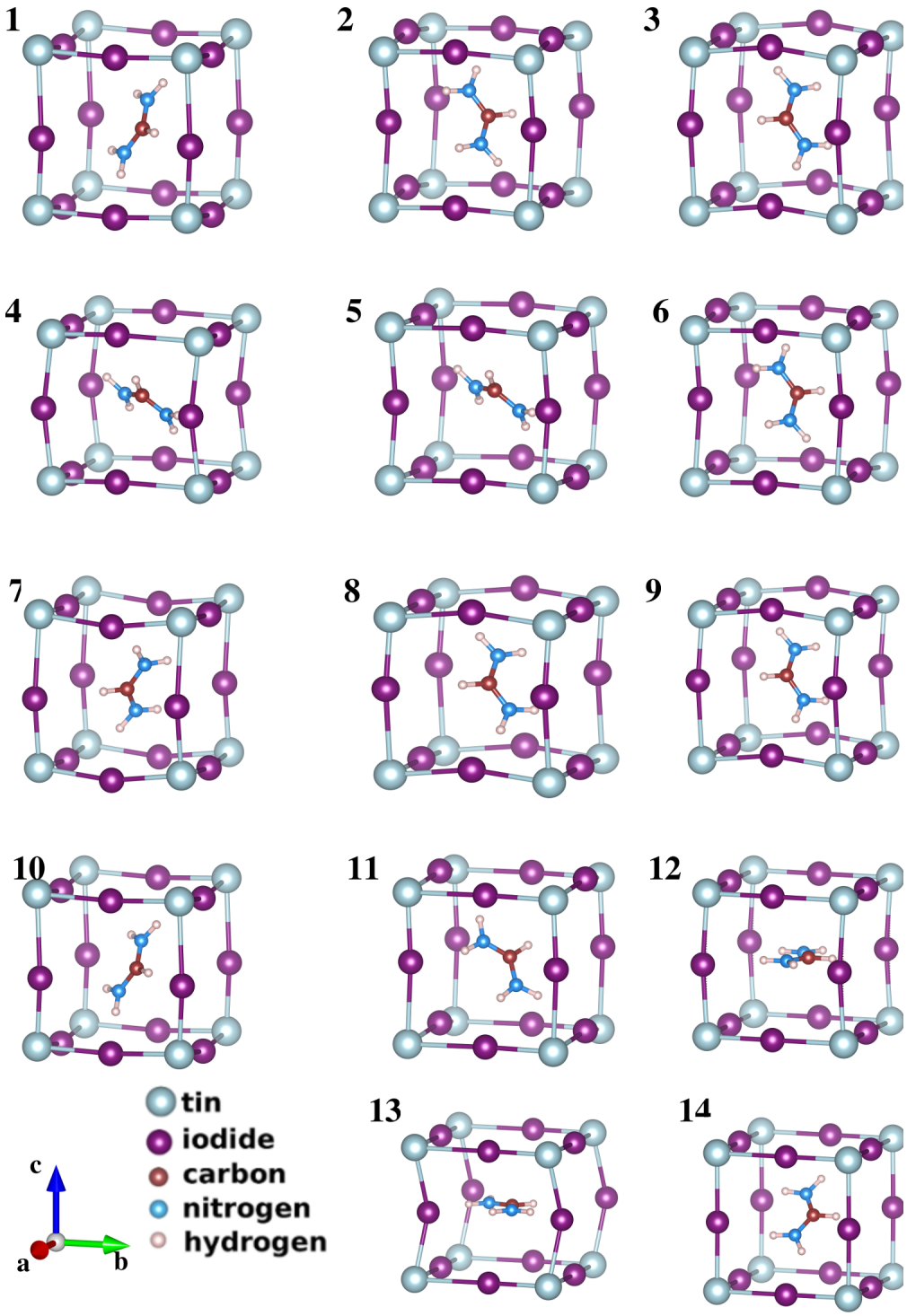

Figure S44 Orientation of organic cation in the pseudo-cubic structures.

Table S36 Lattice parameters of pseudo-cubic phase of $FASnI_3$ perovskite, ($\alpha = \beta = \gamma = 90°$)

N	a_0 (Å)	b_0 (Å)	c_0 (Å)	N	a_0 (Å)	b_0 (Å)	c_0 (Å)
1	6.28	6.29	6.52	**8**	6.29	6.27	6.53
2	6.28	6.29	6.52	**9**	6.30	6.27	6.52
3	6.29	6.28	6.52	**10**	6.28	6.29	6.52
4	6.30	6.52	6.27	**11**	6.21	6.47	6.50
5	6.27	6.52	6.30	**12**	6.40	6.24	6.31
6	6.28	6.30	6.51	**13**	6.53	6.53	6.20
7	6.30	6.27	6.52	**14**	6.41	6.33	6.40

Table S37 Relative total energy (ΔE_{tot}), enthalpy of formation (ΔH_f^o) and cohesive energy (E_{coh}) of each $FASnI_3$ pseudo-cubic structure.

N	ΔE_{tot} (meV/f.u.)	ΔH_f^o (meV/f.u.)	E_{coh} (eV/atom)	N	ΔE_{tot} (meV/f.u.)	ΔH_f^o (meV/f.u.)	E_{coh} (eV/atom)
1	0.00	31.14	−3.68	**8**	0.15	31.30	−3.68
2	0.00	31.15	−3.68	**9**	0.17	31.31	−3.68
3	0.02	31.16	−3.68	**10**	0.20	31.34	−3.68
4	0.06	31.20	−3.68	**11**	27.58	58.72	−3.67
5	0.08	31.22	−3.68	**12**	110.11	141.25	−3.67
6	0.08	31.22	−3.68	**13**	115.90	147.04	−3.67
7	0.10	31.24	−3.68	**14**	138.88	170.02	−3.67

7.3 Orthorhombic structures of $FASnI_3$ perovskites

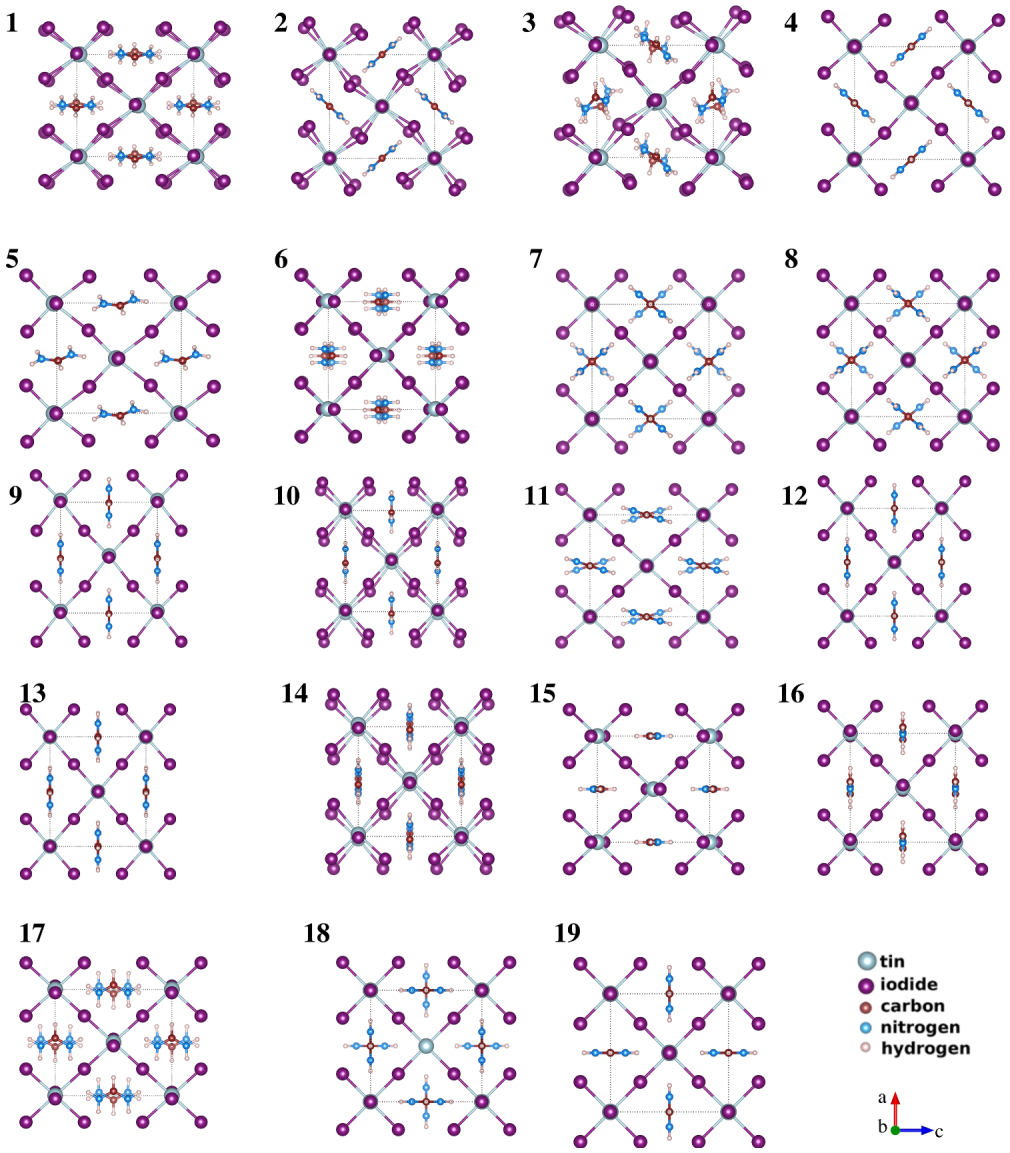

Figure S45 Orientation of organic cation in the orthorhombic structures.

Table S38 Lattice parameters of othorhombic phase of $FASnI_3$ perovskite, ($\alpha = \beta = \gamma = 90°$).

N	a_0 (Å)	b_0 (Å)	c_0 (Å)	N	a_0 (Å)	b_0 (Å)	c_0 (Å)
1	8.40	12.52	9.63	**11**	8.45	12.50	9.40
2	8.79	12.37	8.90	**12**	9.51	12.54	8.32
3	8.72	12.53	9.05	**13**	9.50	12.54	8.33
4	8.89	12.42	8.95	**14**	9.13	12.89	8.57
5	8.45	12.55	9.51	**15**	8.54	12.75	9.04
6	8.90	12.82	8.86	**16**	8.99	12.86	8.68
7	8.86	12.47	9.03	**17**	8.54	12.56	9.38
8	8.82	12.47	9.06	**18**	9.05	12.71	9.04
9	9.56	12.57	8.35	**19**	9.08	12.63	9.08
10	9.31	12.62	8.48				

Table S39 Relative total energy (ΔE_{tot}), enthalpy of formation (ΔH_f^o) and cohesive energy (E_{coh}) of each $FASnI_3$ orthorhombic structure.

N	ΔE_{tot} (meV/f.u.)	ΔH_f^o (meV/f.u.)	E_{coh} (eV/atom)	N	ΔE_{tot} (meV/f.u.)	ΔH_f^o (meV/f.u.)	E_{coh} (eV/atom)
1	0.00	−48.14	−3.68	**11**	75.01	26.88	−3.68
2	2.63	−45.50	−3.68	**12**	75.12	26.98	−3.68
3	13.91	−34.23	−3.68	**13**	75.89	27.76	−3.68
4	25.25	−22.88	−3.68	**14**	78.88	30.75	−3.68
5	28.32	−19.82	−3.68	**15**	128.50	80.36	−3.67
6	31.28	−16.86	−3.68	**16**	173.47	125.33	−3.67
7	46.96	−1.18	−3.68	**17**	192.61	144.47	−3.67
8	51.34	3.20	−3.68	**18**	219.93	171.79	−3.67
9	64.75	16.61	−3.68	**19**	261.66	213.52	−3.66
10	66.63	18.49	−3.68				

7.4 Tetragonal structures of $FASnI_3$ perovskites

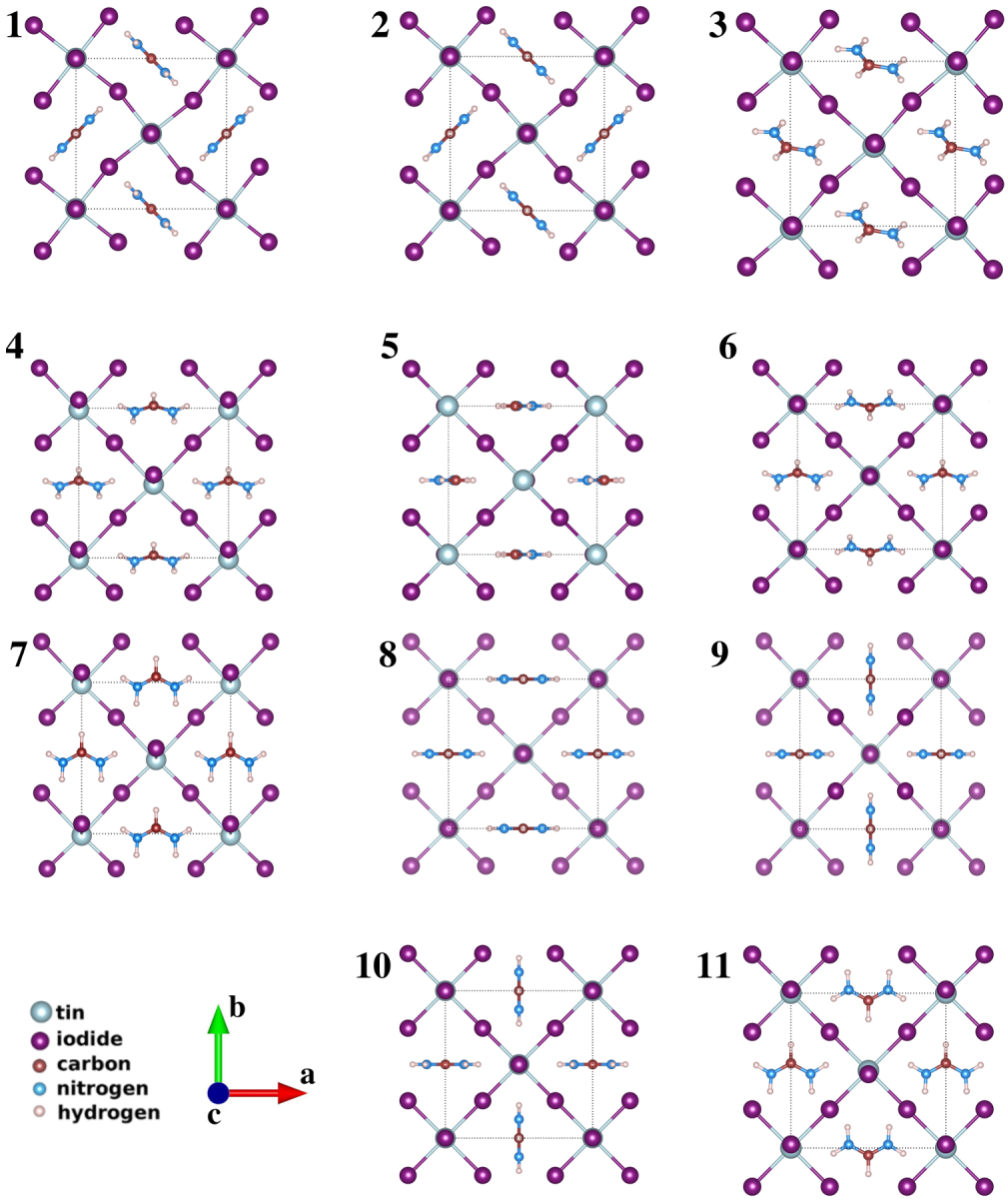

Figure S46 Orientation of organic cation in the tetragonal structures.

Table S40 Lattice parameters of tetragonal phase of $FASnI_3$ perovskite, ($\alpha = \beta = \gamma = 90°$).

N	a_0 (Å)	b_0 (Å)	c_0 (Å)	N	a_0 (Å)	b_0 (Å)	c_0 (Å)
1	8.88	8.88	6.19	**7**	9.23	9.23	6.20
2	8.92	8.92	6.20	**8**	9.05	9.05	6.32
3	8.97	8.97	6.33	**9**	9.08	9.08	6.32
4	9.17	9.17	6.22	**10**	9.09	9.09	6.24
5	8.80	8.80	6.64	**11**	9.07	9.07	6.23
6	9.08	9.08	6.26				

Table S41 Relative total energy, ΔE_{tot}, enthalpy of formation, ΔH_f^o, and cohesive energy, E_{coh}, of each $FASnI_3$ tetragonal structure.

N	ΔE_{tot} (meV/f.u.)	ΔH_f^o (meV/f.u.)	E_{coh} (eV/atom)	N	ΔE_{tot} (meV/f.u.)	ΔH_f^o (meV/f.u.)	E_{coh} (eV/atom)
1	0.00	−34.36	−3.68	**7**	180.23	145.87	−3.67
2	11.34	−23.02	−3.68	**8**	200.38	166.02	−3.67
3	71.48	37.13	−3.68	**9**	247.73	213.37	−3.66
4	92.68	58.32	−3.67	**10**	261.27	226.91	−3.66
5	102.09	67.74	−3.67	**11**	298.32	263.97	−3.66
6	125.90	91.55	−3.67				

7.5 Pseudo-hexagonal structures of $FASnI_3$ perovskites

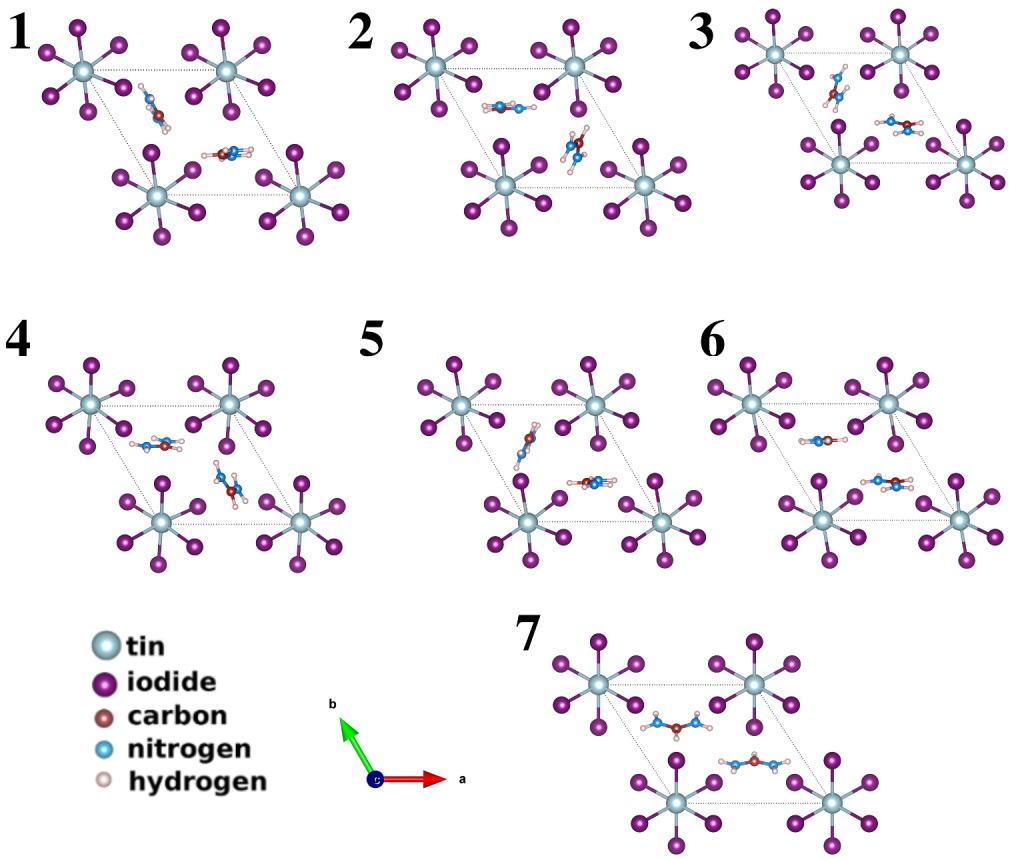

Figure S47 Orientation of organic cation in the pseudo-hexagonal structures.

Table S42 Lattice parameters of pseudo-hexagonal phase of $FASnI_3$ perovskite.

N	a_0 Å	b_0 Å	c_0 Å	α deg	β deg	γ deg	N	a_0 Å	b_0 Å	c_0 Å	α deg	β deg	γ deg
1	8.52	8.64	7.91	86.36	92.15	120.62	**5**	8.53	8.57	7.90	92.84	91.19	119.57
2	8.64	8.55	7.87	87.32	94.43	120.47	**6**	8.65	8.60	7.93	91.21	87.04	121.41
3	8.54	8.76	7.83	94.11	87.71	120.92	**7**	9.51	8.67	7.47	93.42	90.00	123.24
4	8.72	8.64	7.81	84.79	94.73	121.20							

Table S43 Relative total energy, ΔE_{tot}, enthalpy of formation (ΔH_f^o) and cohesive energy (E_{coh}) of each $FASnI_3$ pseudo-hexagonal structure.

N	ΔE_{tot} (meV/f.u.)	ΔH_f^o (meV/f.u.)	E_{coh} (eV/atom)	N	ΔE_{tot} (meV/f.u.)	ΔH_f^o (meV/f.u.)	E_{coh} (eV/atom)
1	0.00	−46.09	−3.68	**5**	4.15	−41.93	−3.68
2	0.07	−46.02	−3.68	**6**	15.79	−30.29	−3.68
3	1.98	−44.10	−3.68	**7**	111.13	65.04	−3.67
4	3.41	−42.67	−3.68				

7.6 Hexagonal structures of $FASnI_3$ perovskites

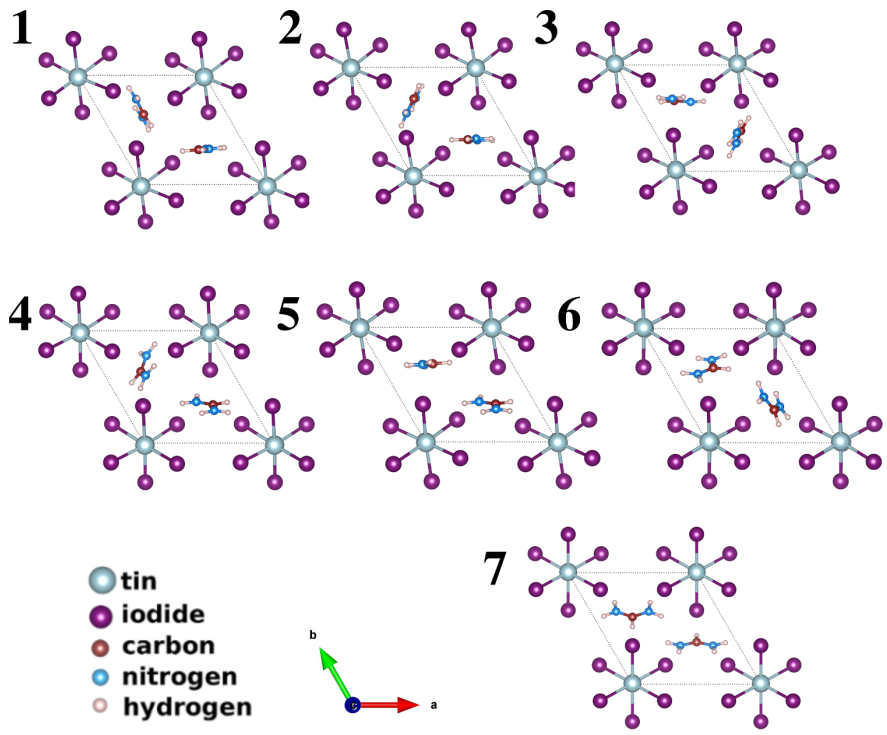

Figure S48 Orientation of organic cation in the hexagonal structures.

Table S44 Lattice parameters of hexagonal phase of $FASnI_3$ perovskite.

N	a_0 Å	b_0 Å	c_0 Å	α deg	β deg	γ deg	N	a_0 Å	b_0 Å	c_0 Å	α deg	β deg	γ deg
1	8.58	8.58	7.85	90.00	90.00	120.00	**5**	8.62	8.62	7.81	90.00	90.00	120.00
2	8.55	8.55	7.91	90.00	90.00	120.00	**6**	8.68	8.68	7.67	90.00	90.00	120.00
3	8.60	8.60	7.81	90.00	90.00	120.00	**7**	9.09	9.09	7.18	90.00	90.00	120.00
4	8.65	8.65	7.74	90.00	90.00	120.00							

Table S45 Relative total energy, ΔE_{tot}, enthalpy of formation, ΔH_f^o, and cohesive energy, E_{coh}, of each $FASnI_3$ hexagonal structure.

N	ΔE_{tot} (meV/f.u.)	ΔH_f^o (meV/f.u.)	E_{coh} (eV/atom)	N	ΔE_{tot} (meV/f.u.)	ΔH_f^o (meV/f.u.)	E_{coh} (eV/atom)
1	0.00	−25.31	−3.68	**5**	15.91	−9.41	−3.68
2	4.35	−20.96	−3.68	**6**	26.86	1.55	−3.68
3	5.55	−19.76	−3.68	**7**	202.48	177.17	−3.66
4	6.06	−19.25	−3.68				